DETECTION AND QUANTIFICATION OF RARE ANALYTES IN BIOLOGICAL SAMPLES USING DIELECTROPHORETIC SPECTROSCOPY

A Dissertation
Submitted to the Graduate Faculty
of the
North Dakota State University
of Agriculture and Applied Science

By

Syed Abdul Mannan Kirmani

In Partial Fulfillment of the Requirements
for the Degree of
DOCTOR OF PHILOSOPHY

Major Department:
Electrical and Computer Engineering

December 2016

Fargo, North Dakota

North Dakota State University
Graduate School

Title

Detection and quantification of rare analytes in biological samples using dielectrophoretic spectroscopy

By

Syed Abdul Mannan Kirmani

The Supervisory Committee certifies that this ***disquisition*** complies with North Dakota State University's regulations and meets the accepted standards for the degree of

DOCTOR OF PHILOSOPHY

SUPERVISORY COMMITTEE:

Ivan T. Lima Jr.
Chair

David Rogers

Sherif Sherif

Sumathy Krishnan

Approved:

December 12, 2016
Date

Scott C. Smith
Department Chair

ABSTRACT

Novel techniques for Dielectrophoresis (DEP) crossover frequency calculation, positive dielectrophoretic spectroscopy and negative dielectrophoretic spectroscopy are proposed in this dissertation. A novel automated immunoassay based on negative dielectrophoretic spectroscopy for the detection and quantification of rare-analytes in a biological sample is also presented. All of these techniques are based on a custom made automated software "*DEP spectroscopy application*" for Microsoft Windows that was designed and developed for this research project. The techniques for DEP crossover frequency calculation and dielectrophoretic spectroscopy were validated through experiments with blue colored polystyrene beads with 1000 nm diameter. The techniques for positive dielectrophoretic spectroscopy and negative dielectrophoretic spectroscopy were validated through experiments with fluorescent polystyrene beads with 500 nm diameter. An increase in negative DEP force was observed in response to the increase in the frequency of the applied electric field. This increased DEP force resulted in higher speed of repulsion of functionalized polystyrene beads from the edge of the electrode. The speed of repulsion was measured for 0%, 0.8%, 50% and 100% conjugation of avidin with biotin functionalized polystyrene beads with the automated software through real-time image processing. A significant difference in the velocity of the beads was observed among different avidin-biotin conjugation concentrations that can be used to quantify rare analytes in a biological sample. Using this technique, as little as 80 molecules of avidin per biotin functionalized bead can be detected in a sample. This technology can be applied to the detection and quantification of rare analytes that can be useful in the diagnosis and treatment of diseases like cancer and myocardial infarction with the use of polystyrene beads functionalized with antibodies for the target biomarkers.

ACKNOWLEDGEMENTS

I want to thank Allah for all of His blessings that enabled me to complete this research. I would not be able to complete it without the guidance and help of my mentor and advisor Dr. Ivan Lima. He guided me with kindness and keen interest and always provided me with valuable feedback to achieve my goals. I am also greatly indebted to all the respected members of my supervisory committee, Dr. David Rogers, Dr. Sherif Sherif and Dr. Sumathy Krishnan for their kind help and support throughout my research. I am thankful to Dr. Dharmakeerthi Nawarathna for his great help, support and kind feedback throughout my research. I want to thank all my teachers, Dr. Benjamin Braaten, Dr. Debasis Dawn, Dr. Rajesh Kavasseri, Dr. Orven Swenson and Dr. Scott Smith who helped me a lot in my professional and academic development. I am also thankful to all my colleagues, Logeeshan Velmanickam, Fleming Gudagunti, Anshul Kalra, Thiago De Menezes and Alexandre Yamamoto for their kind help and support in achieving my goals. I am also grateful to Mr. Jeffrey Erickson, Ms. Laura Dallmann, Ms. Priscilla Schlenker, Ms. Betsy Carter, Mr. Paul Omernik and Ms. Patty Hartsoch for their kind help and support throughout my stay at NDSU. In the end, I want to thank my parents, my wife and my children for their unconditional love and support.

I also want to express my profound gratitude to COMSATS Institute of Information Technology (CIIT), Islamabad, Pakistan, for the award of academic scholarship for graduate studies at NDSU. I am indebted to all my senior mentors at CIIT for providing me this opportunity that enabled me to pursue my higher education in a good university in the United States.

DEDICATION

To my mother, my father, my sisters, my wife, my children and all the family members for their kind prayers, unconditional love and support

TABLE OF CONTENTS

LIST OF FIGURES

Figure Page

1. INTRODUCTION

Early diagnosis is vital for successful treatment of many life-threatening medical conditions[1,2]. Accurate diagnosis of a disease and subsequent prognosis by a physician involves a number of laboratory tests. Because of their inherent importance as lifesaving tools, medical laboratory tests should satisfy a set of stringent quality standards and requirements. The most basic of which is the reliability. There is a growing need to produce reliable results in a cost effective and time saving manner using a small volume of the test sample. To cater to this demand, a lot of research is being done on the development of very small sensors (sizes on order of μm) and lab-on-chip devices. Many laboratory tests involve detecting and quantifying some rare analyte in the biological sample through a biosensor[3].

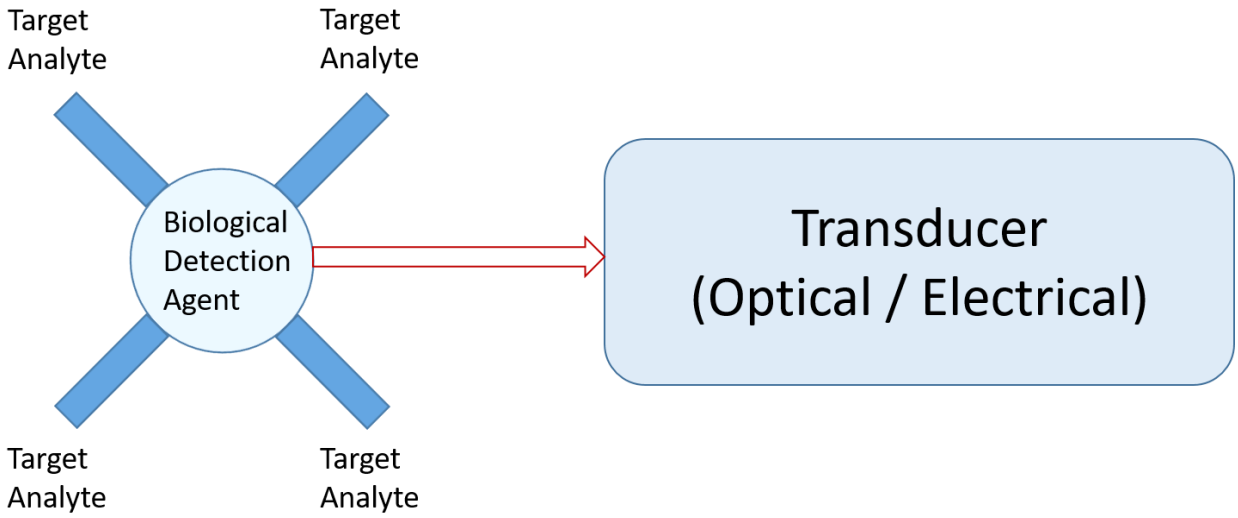

Fig. 1. Block diagram of a biosensor

A biosensor essentially consists of a sensitive biological element, which reacts selectively with the target analyte and a transducer or detector with associated signal processing and output display as shown in Fig. 1[4]. The biosensors use a biomolecule like an enzyme, protein, antibody, nucleic acid, etc., as an active detection agent[3–5]. Broadly, biosensors are categorized into either catalytic or affinity biosensors[4]. The catalytic biosensors employ an active biomolecule like an

enzyme that reacts specifically with some rare analytes[4]. The affinity biosensors exploit the specific interaction of an analyte (ligand) and a biological receptor[4]. An immunosensor is essentially an affinity biosensor that exploits antibody-antigen interactions[6–8]. Antibodies are glycoprotein molecules called immunoglobulins that are produced by plasma cells as an immune response induced by an antigen[4]. When incorporated into a biosensor, the antibody is either adsorbed or covalent bonded to a solid surface like a polystyrene well plate as in case of Enzyme Linked Immunosorbent Assay (ELISA) or to polystyrene beads as in Latex Agglutination Assay (LA)[3,5,7,9]. Then, the biological sample containing the target analytes is either pipetted, flowed or mixed with the immunoassay[5,10]. Any antigen molecules present in the sample react readily with the antibody in the assay and agglutination occurs[11,12]. There are many different techniques to detect and quantify the agglutination in LA and ELISA like dielectrophoresis (DEP) or electrochemical impedance spectroscopy[13–18]. In DEP various target biological particles like antigens, antibodies, cells or DNA can be detected, isolated, concentrated or purified[4,19–21]. Mostly visual inspection is done to detect positive or negative DEP regions or crossover frequencies[5], but recently automated procedures have also been reported for detection and quantification of DEP forces and crossover frequencies[22–27]. Suehiro *et al.* proposed a dielectrophoretic impedance measurement method for quantitative estimation of biological cell concentrations suspended in aqueous medium[22]. However, impedance measurement requires expensive impedance analyzers and the results vary with the conductance of the analyte and the biological sample[5]. Song *et al.* proposed an approach based on artificial neural networks for quantification of dielectrophoretic force that is computationally intensive[23]. Bakewell *et al.* used statistical image quantification methods for evaluation of surface conductance and conductivity of nanoparticles with positive DEP experiments[27]. The drawback of their approach includes complexity of the involved image

processing techniques. Wei et al. and Pesce et al. employed techniques based on optical tweezers for dielectrophoretic force measurements[25,26]. Optical tweezers are very sensitive measurement devices and require extensive and careful calibration. The method proposed in this dissertation efficiently measures the effect of the DEP force through a live video feed from the microscope camera and performs real-time image processing. It records the change in the fluorescence emission as the system automatically scans the electric frequency of the function generator over a specified time interval. The effectiveness of the method was demonstrated by extracting the crossover frequencies and the DEP spectrum of polystyrene beads with blue color dye (1000 nm diameter) and green fluorescent polystyrene beads with 500 nm diameter using this procedure. This approach can lead to the development of detection methods with significantly higher sensitivity than existing detection methods. Velmanickam et.al.[5] reported a dielectrophoretic label-free immunoassay for rare analyte quantification in biological samples with capability to detect and quantify about 850 avidin molecules attached to biotin functionalized polystyrene beads. An improved method is proposed in this dissertation in which the quantitative measurement of DEP through image processing is automated and DEP spectroscopic curves for various concentrations of biotin-avidin conjugates over a range of frequencies are obtained. These standard curves can be utilized to detect and quantify avidin molecules in biological samples. This technique resulted in an improvement by an order of magnitude in the detection limit of rare analytes from previous published results[5]. This method based on DEP spectroscopy has the potential to be used as a primary point of care diagnostic technique because of its use of very small electrodes (size on the order of μm) and its capability to detect very low concentration of target analytes (< pg/ml). The quantification of rare analytes is of much importance for detecting various stages of tumors in oral and prostate cancer[1,2,5]. Similarly, early detection of raised troponin level in blood can help in

diagnosis and treatment of myocardial infarction[28–30]. For detection of other rare analytes, this technique can be modified by substituting biotin with another binding antibody for the respective target analyte.

2. ELECTROKINETICS

Electrokinetics deals with the motion of micro or nanoscale particles (either charged or neutral) suspended in a fluid under the influence of an electric field[20,31,32].

2.1. Electrical Double Layer

When an electrode is immersed in an electrolyte or a charged particle is suspended in an ionic solution, an electrical double layer is formed at the solid – liquid interface[4]. The formation of this layer is explained in Fig. 2.

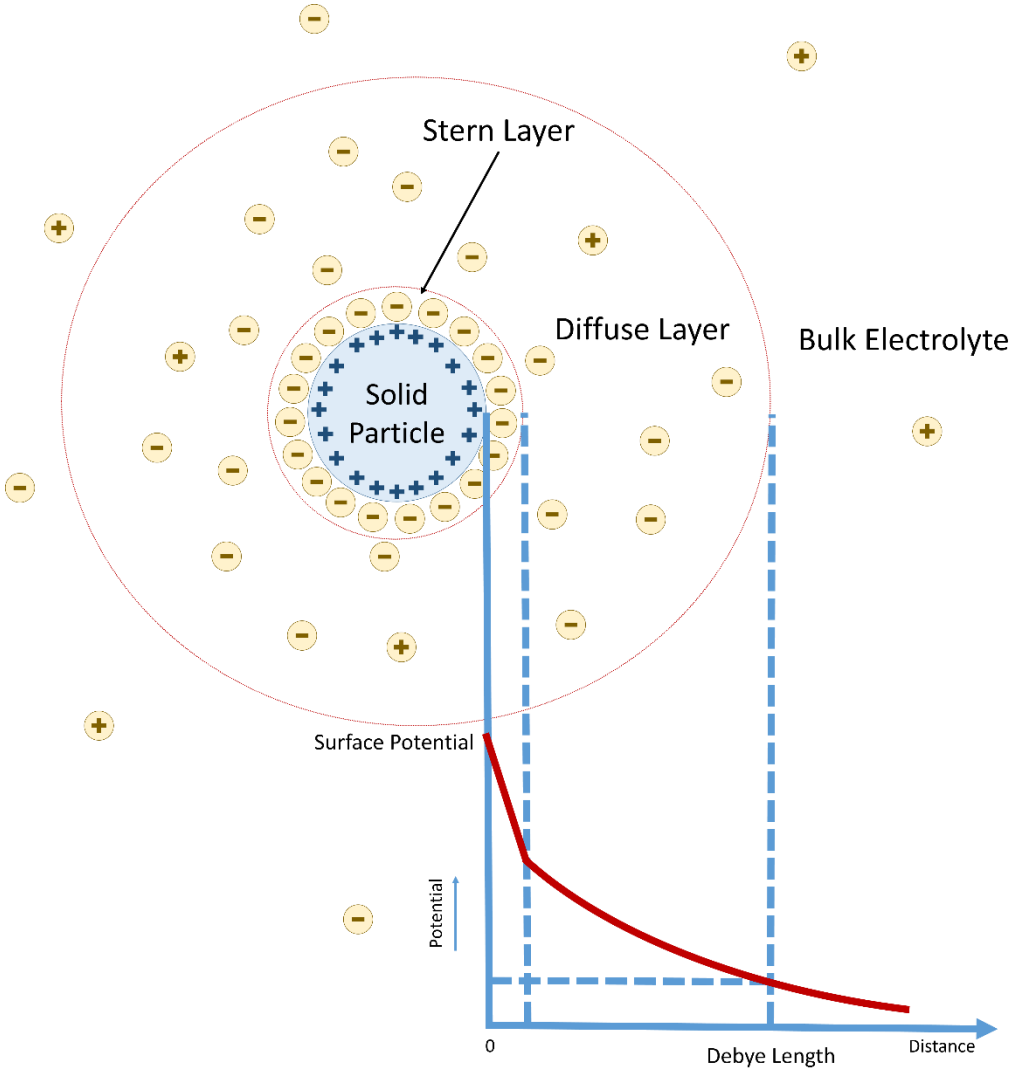

Fig. 2. Electrical Double Layer (assuming solid particle has positive charge)

Ions opposite in charge to the solid surface surround the immersed electrode or suspended particle and form a layer, known as Stern layer[33]. Ions in the Stern layer are adsorbed to the surface and are closely packed. The electric potential drops linearly across the Stern layer. More ions from the electrolyte form a layer of loosely bound ions beyond the Stern layer within a distance corresponding to the Debye length[4,34]. The second layer is known as the diffuse layer. The potential drops exponentially across the diffuse layer. The interface between the diffuse layer and the bulk electrolyte solution is called the slip plane. The potential at the slip plane is called zeta potential. The Debye length is given by the relation[4,33–35]:

$$L_d = \sqrt{\frac{\varepsilon_o \varepsilon_m kT}{8\pi N_0 Z^2 q^2}}, \tag{2.1}$$

where ε_o is the permittivity of the free space, $\varepsilon_m$is the relative permittivity of the medium, k is the Boltzmann constant, T is the absolute temperature, N_0 is the bulk concentration of ions in the electrolyte, Z is the valency of the electrolyte and q is the charge on an electron. The charged surface is electrically screened beyond the Debye length from the bulk electrolyte solution[4]. Because of the formation of electrical double layer, ions in the electrolyte are attracted towards the solid particles or surfaces and their concentration is increased in those areas. That is why, the concentration of ions near the particle or electrode exceeds N_0 which is the bulk concentration of ions in the electrolyte[34].

2.2. Dielectrophoresis

Dielectrophoresis (DEP) is an electrokinetic phenomena in which electrically neutral polarizable particles move in a non-uniform electric field[4,36]. It is exploited in biotechnology for its remarkable capability of selectively isolating, concentrating or purifying target bio particles present within a complex mixture by either attracting or repelling these target bio particles from

the electrodes[19,37,38]. The translational forces of attraction or repulsion arise from the interaction of the dipole moment of the particles with the non-uniform electric field[39]. Electrodes of different lengths or complex shapes create a non-uniform electric field. A high electric field region is created close to the right electrode and a low electric field region is created close to the left electrode as shown in the Fig. 3.

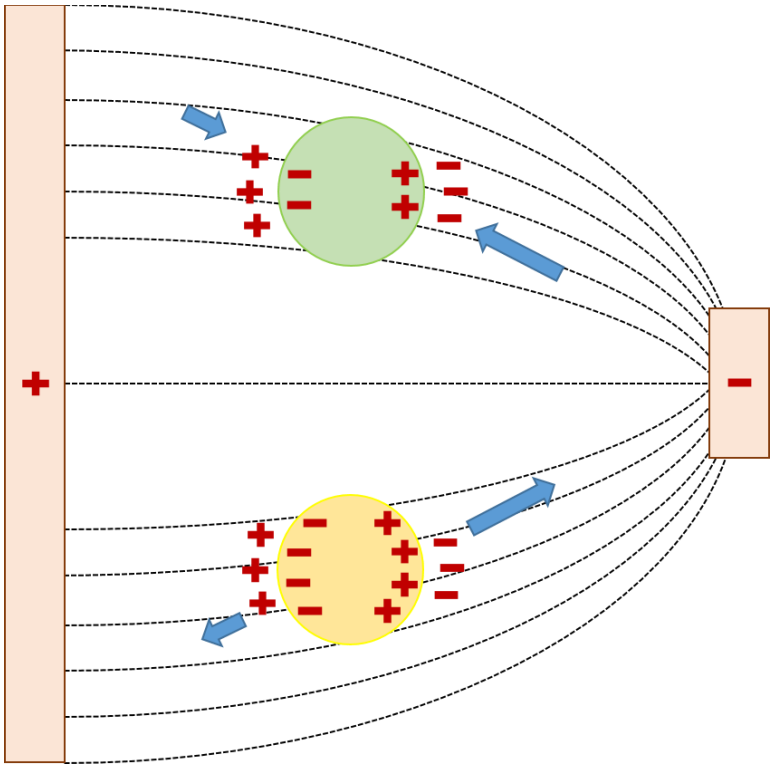

Fig. 3. Dielectrophoresis of a particle in a non-uniform electric field

If the particle is more polarizable than the surrounding medium it experiences a net force towards the high electric field region and will be attracted towards the right electrode. This is called positive DEP. On the other hand, if the particle is less polarizable than the surrounding medium it moves toward the low electric field region. This process is known as negative DEP[40–42]. The time averaged DEP force on a spherical particle of radius r is given by[4,5,19,36]:

$$\langle F_{\mathrm{DEP}} \rangle = 2\pi\varepsilon_o\varepsilon_m r^3 Re[K_{CM}(\omega)]\nabla(E^2), \qquad (2.2)$$

where ε_o is the permittivity of the free space, $\varepsilon_m$is the relative permittivity of the medium, ∇E is the electric field gradient and $Re[K_{CM}(\omega)]$is the real part of the Clausius-Mossotti factor (that is effective polarisability (per unit volume) of the particle) which is given by[4,5,19,36]:

$$K_{CM}(\omega) \equiv \frac{\varepsilon_p^* - \varepsilon_m^*}{\varepsilon_p^* + 2\varepsilon_m^*}, \tag{2.3}$$

where ε_p^* is the complex permittivity of the particle and ε_m^* is the complex permittivity of the medium. The complex permittivity is related to the conductivity σ and the angular frequency ω of the applied alternating current (AC) field through the following relation[4,5,19,36]:

$$\varepsilon^* \equiv \varepsilon - j\frac{\sigma}{\omega}. \tag{2.4}$$

Depending on the relative values of the permittivity of the particle and the medium, the value of $K_{CM}(\omega)$ varies from –0.5 to 1. If $K_{CM}(\omega)$ is positive, then particles are attracted to regions of high electric field intensity, an effect called positive DEP. Similarly, if $K_{CM}(\omega)$ is negative, then the particles are repelled from the regions of high electric field intensity, an effect called negative DEP. Since $K_{CM}(\omega)$ is frequency dependent, both positive and negative DEP effects can be observed by changing the frequency of the applied electric field. The crossover frequency f_{xo} is defined as the frequency at which the force changes from positive to negative DEP. It is given by[4,5,19,36,43]:

$$f_{xo} = \frac{1}{2\pi}\sqrt{-\frac{(\sigma_p - \sigma_m)(\sigma_p + 2\sigma_m)}{(\varepsilon_p - \varepsilon_m)(\varepsilon_p + 2\varepsilon_m)}}, \tag{2.5}$$

where σ and ε are conductivity and the permittivity of the particle and the medium. The value of f_{xo} depends on the conductivity of the particle σ_p at low frequencies (< 1 MHz) and on the permittivity of the particle at higher frequencies. The total conductivity σ_p of a spherical dielectric particle is given by the sum of its bulk σ_{bulk} and surface conductivity K_s [4,5,19,36].

$$\sigma_p = \sigma_{\text{bulk}} + \frac{2K_s}{r}. \quad (2.6)$$

Since σ_{bulk} of the very small particles is negligible, the σ_p is mainly dependent on K_s. Depending on the size and conjugation of the polystyrene beads, the value of K_s can vary over one order of magnitude and provide a means to isolate, concentrate or separate different types of target bio particles[44–47].

2.3. Drag Force

The motion of the particles suspended in the medium is also affected by the drag force due to the friction in the medium[48]. The drag force acting on a small particle moving in a fluid is given by the following relation[49,50]:

$$F_{\text{drag}} = 6\pi\eta r v, \quad (2.7)$$

where η is the viscosity of the medium, r is the radius of the particle and v is the velocity of the particle. The drag force arises because of the friction of the fluid to the motion of the particle and is opposite in direction to DEP force.

2.4. Electrothermal Forces

There is a high electric field generated to manipulate the micro or nano particles by the electrodes whose dimensions are in μm. This high electric field in a very small area generates a lot of heat that is dissipated in the fluid adjacent to the electrode. The power generated by an electric field E per unit volume in the surrounding medium is given by[42]:

$$P_{\text{medium}} = \sigma E^2 \ (\text{W m}^{-3}), \quad (2.8)$$

where σ is the conductivity of the fluid surrounding the electrode.

Similarly, the power dissipated by the electrode is given by the following equation[42]:

$$P_{\text{electrode}} = \frac{V_{\text{rms}}^2}{R}, \tag{2.9}$$

where V_{rms} is the applied root-mean square voltage and R is the resistance of the electrode. The total power dissipation is the sum of these two quantities given by eq. 2.7 and eq. 2.8. This power dissipation in a small volume give rise to an increase in temperature of the sample. The change in temperature ΔT of the sample is approximated by the following relation[42]:

$$\Delta T \approx \frac{\sigma V_{\text{rms}}^2}{k}, \tag{2.10}$$

where V_{rms} is the applied root-mean square voltage, σ is the electrical conductivity of the medium and k is the thermal conductivity of the medium.

Since DEP requires non-uniform electrical field, the power dissipation and resultant temperature change is also non-uniform throughout the sample. This non-uniform temperature changes through the sample volume give rise to local changes in permittivity, conductivity, viscosity and density of the medium[42]. These differences give rise to buoyancy and electro-thermal forces like the Coulomb force and the dielectric force. The Coulomb force arises because of the free volume charges produced as a result of conductivity gradient generated in the fluid[42]. The dielectric force arise because of the differences in permittivity across the volume of the fluid[42].

2.5. Buoyancy

The buoyancy force arises because of the temperature gradient in the fluid giving rise to changes in the density across the fluid which result in natural convection. The buoyancy force is given by[42]:

$$F_B = \frac{\delta \rho_m}{\delta T} \Delta T g, \tag{2.11}$$

where ρ_m is the density of the medium, T is the temperature and g is acceleration due to gravity.

2.6. Brownian Motion

The time averaged movement of a particle undergoing Brownian motion is zero. The force due to the Brownian motion on an isolated colloidal particle (experiencing no other phenomenon) is given by[42]:

$$F_{\text{Brownian}}(t) = m\frac{\delta v}{\delta t} + 6\pi\eta r v, \tag{2.12}$$

where m is the mass of the particle, v is the velocity of the particle, r is the radius of the particle and η is the viscosity of the medium. The force due to Brownian motion is negligible as compared to the DEP force and does not hinder the movement of colloidal particles because of the DEP[35,42].

3. DEP SPECTROSCOPY APPLICATION

I have developed a Microsoft Foundation Classes (MFC) application in Visual C++ for the Microsoft Windows operating system to carry out DEP spectroscopy of dielectric particles dissolved in a conductive solution. The application can capture live video and time lapse images from any USB Video Class (UVC) standard compliant microscope camera and perform real-time image processing to efficiently measure the effect of the DEP force on dielectric particles and find out the DEP crossover frequency and the DEP spectroscopic curve.

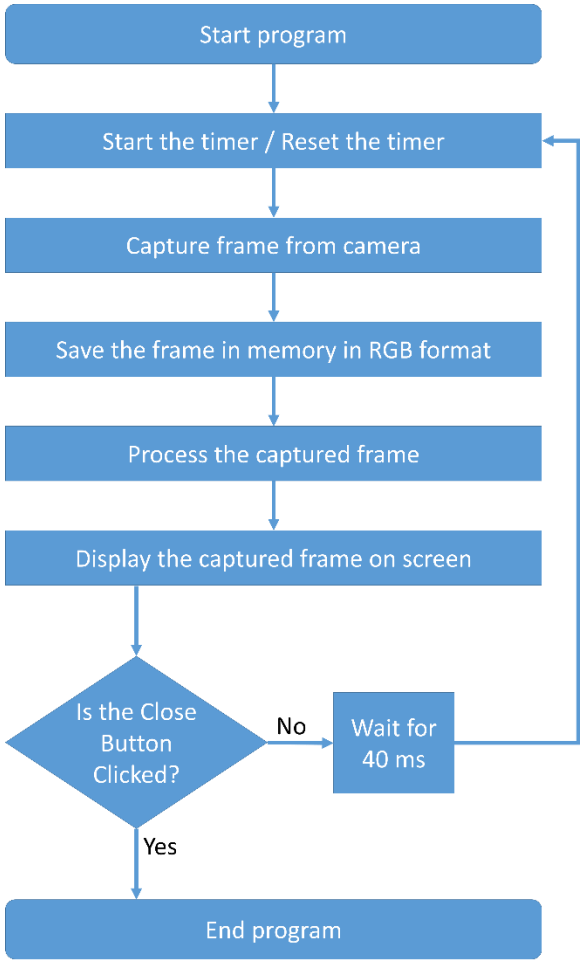

Fig. 4. Simplified flowchart of the DEP spectroscopy application[51]

A simplified flowchart of the program is shown in Fig. 4. The program creates a dialog based MFC application. The UVC standard compliant camera is accessed through Video for

Windows (VfW) library provided by Microsoft. A frame is captured from the camera and saved as a bitmap in memory. The bitmap is processed and converted to a grayscale image. If an experiment is being performed further image processing is done on the grayscale image as per the experimental setup and settings. The results of the experiment and required images are saved in memory. The original captured frame is displayed as shown in Fig. 5. The processed greyscale image is displayed in measurement window shown in Fig. 6. The measurement window provides a host of other functions and settings for the experiment.

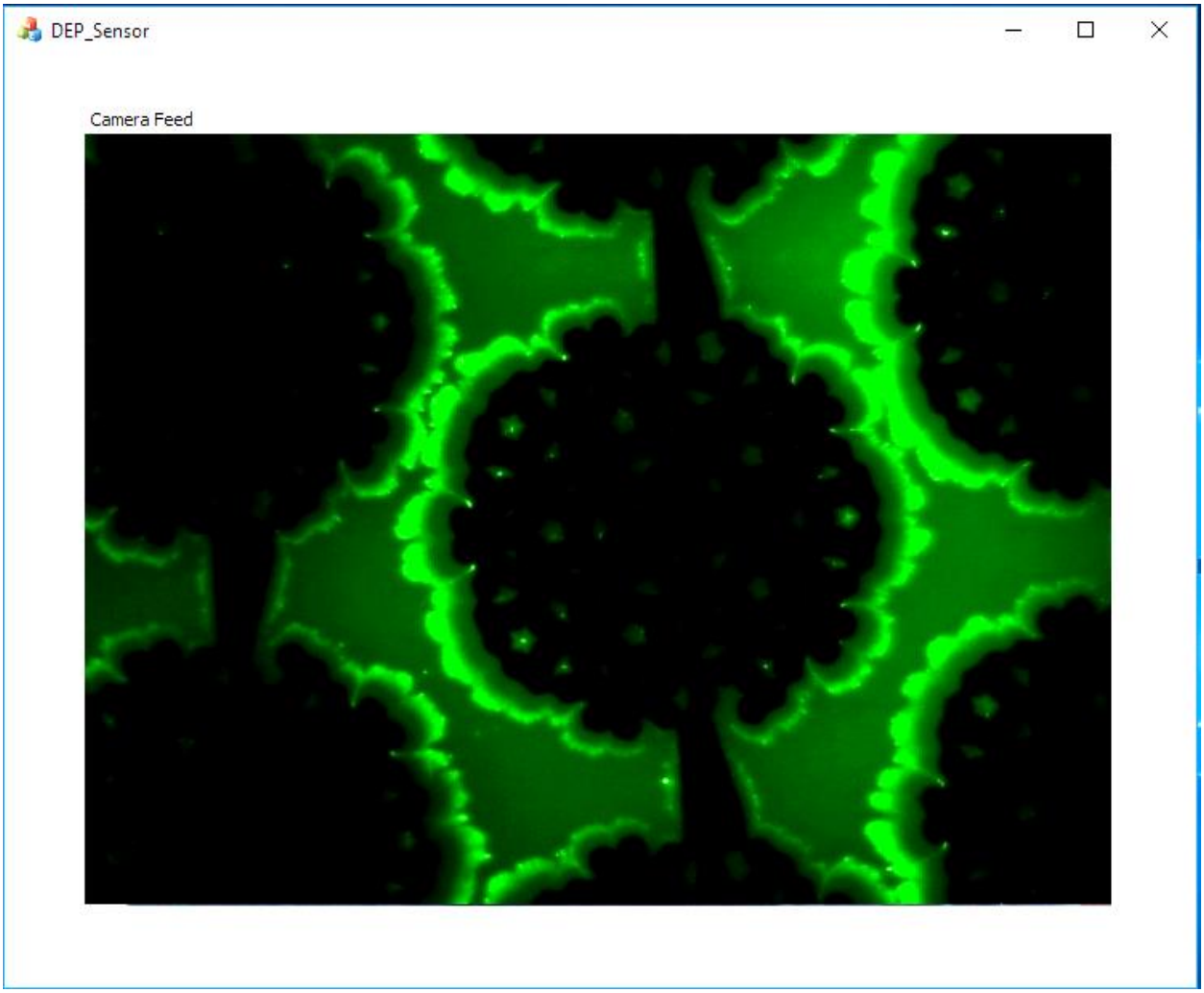

Fig. 5. MFC application for DEP spectroscopy showing live camera feed

The application captures and displays live video from microscope camera with a frame rate of 25 frames per second as shown in Fig. 5. The frame rate can be increased or decreased to a value within hardware constraints. The application then converts the captured frames into greyscale and performs real-time image processing to obtain information about the dynamics. The application has the complete pixel information, including the color, of the captured video frames in computer memory and can perform various real-time image processing tasks to obtain useful information.

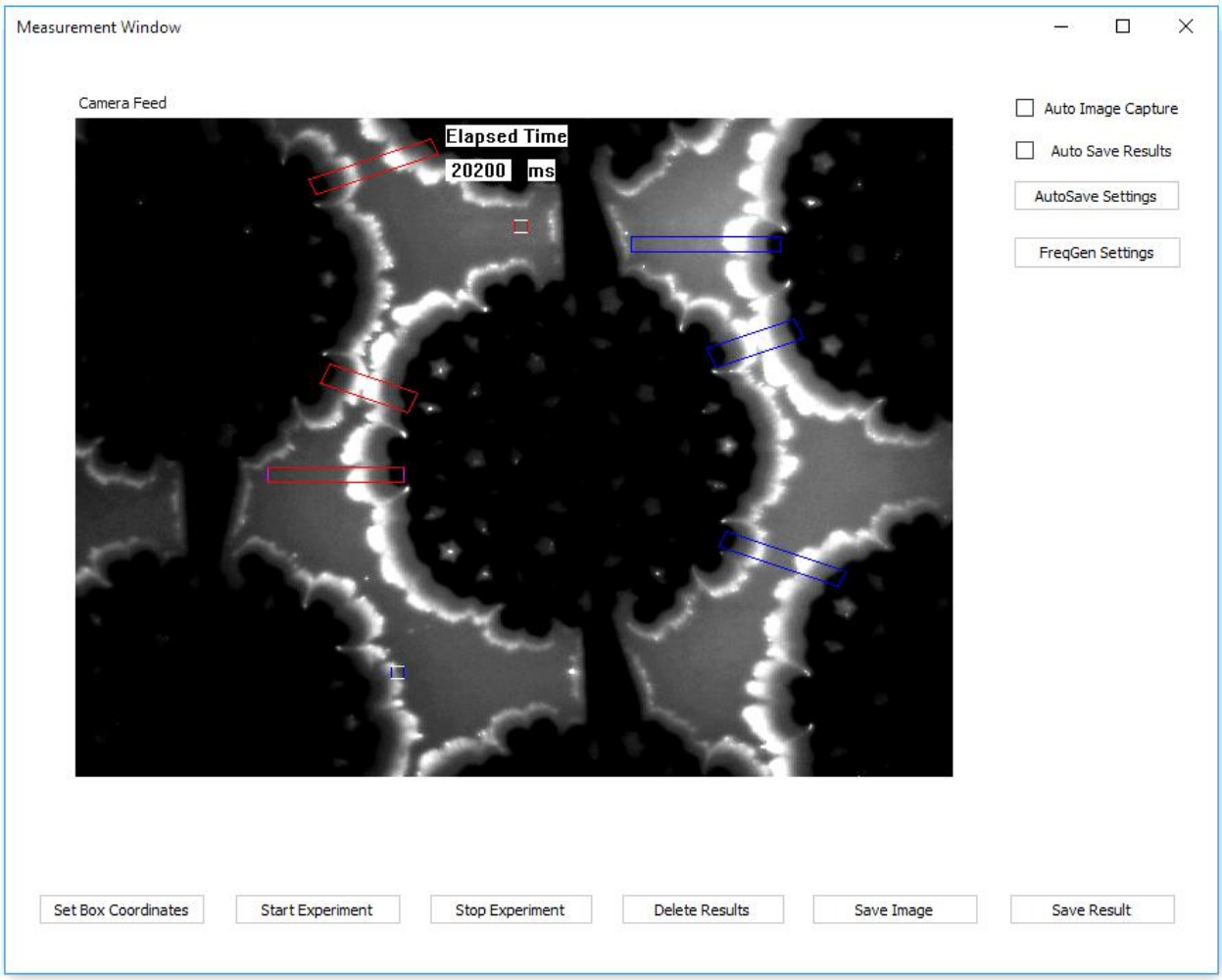

Fig. 6. Measurement Window: displays live greyscale video feed with various options for realtime image analysis[51]

The regions of interest in the video, where a strong DEP effect is visible, are identified to efficiently analyze the effect of the DEP force on the suspended particles in the conductive

medium. Those regions of interest are marked with rectangles, squares, or parallelograms. The image area within these regions of interest is now processed and recorded for efficiently characterizing the DEP force and calculating the DEP spectroscopic curve. The "Set Box Coordinates" button in Fig. 6 displays another dialog window shown in Fig. 7 from where the height, width, slope and position of a square, rectangle or parallelogram can be set to specify the region of interest for the experiment.

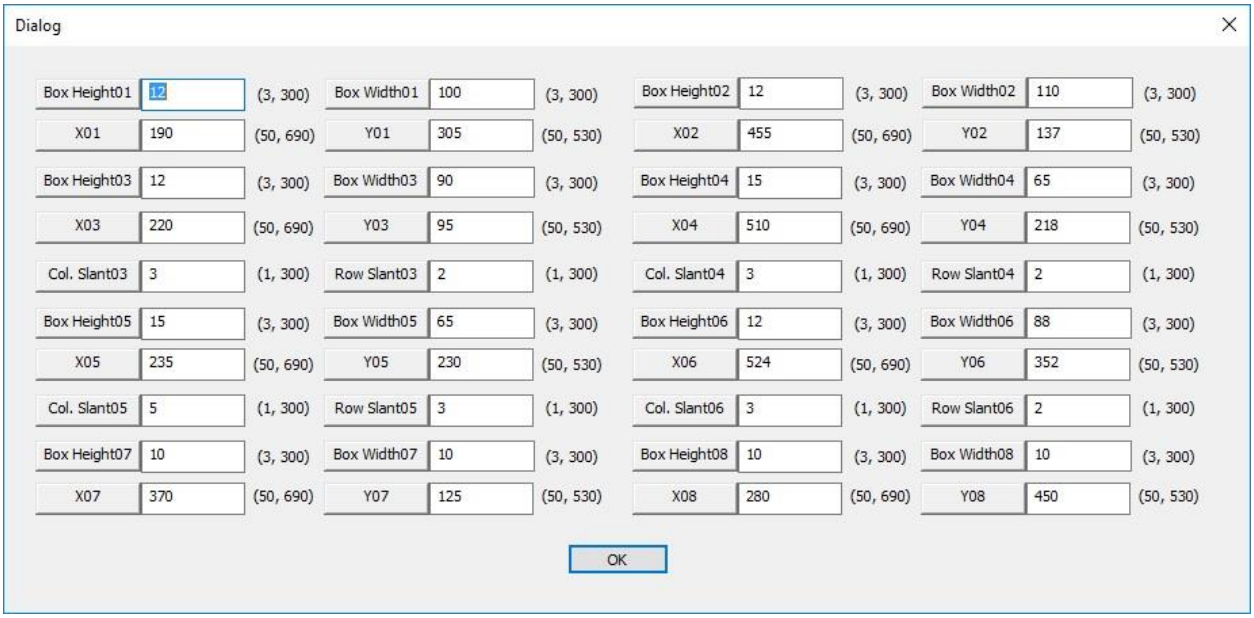

Fig. 7. Dialog window to specify size and position of desired region of interest for the experiment

As shown in Fig. 8, a desired interval to capture time lapse images for further processing and record data values during the experiment can be set by clicking on the "AutoSave Settings" button in Fig. 6. The minimum time interval to capture an image or record a new data value is 40 ms which is determined by the frame rate of the video stream and processing speed of the hardware. Different time intervals for positive and negative DEP analysis can be specified. Since the suspended particles take some time to accumulate along the edges of the electrode when positive DEP is observed, additional time is needed to analyze this effect. However, in case of negative

DEP, the accumulated particles along the edge of the electrode are readily repelled as the frequency is changed. So, negative DEP requires much less time for examination.

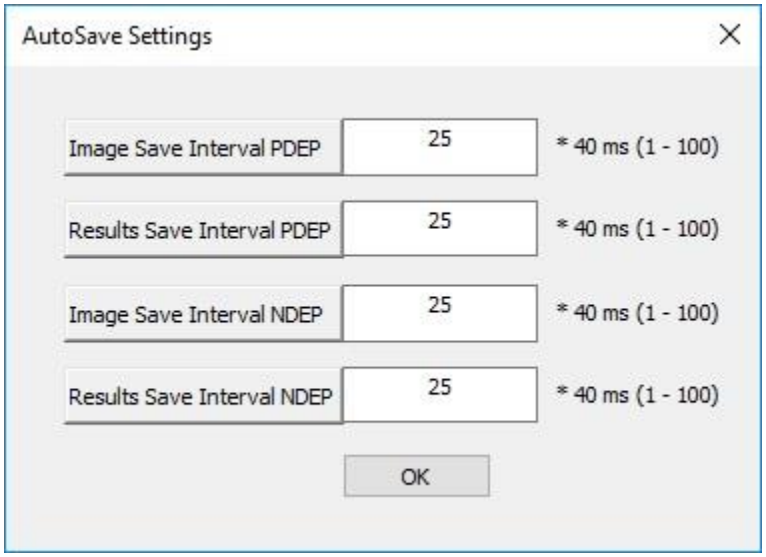

Fig. 8. AutoSave Settings dialog window

The function generator can be set to automatically scan through a set of electrical frequencies over the specified intervals of time. The settings dialog window as shown in Fig. 9 can be opened by clicking on the "FreqGen Settings" button in Fig. 6. The address of the function generator, the start, stop, and step frequency and peak to peak voltage can be specified in this dialog window. Moreover, the time interval for the frequency to induce positive DEP and the time interval for the frequency to induce negative DEP can be specified as well. The experiment can be performed either to observe and analyze positive DEP or the negative DEP. In case of positive DEP, the experiment starts with a frequency to induce positive DEP for the specified time interval. When the time interval elapses, the frequency is automatically changed to another frequency that induces negative DEP for the specified time interval. Then, the positive frequency is incremented by the frequency step size. This cycle goes on until the stop frequency is reached. All frequency switching by the function generator is done automatically by the application. The application is designed for Tektronix AFG series function generators. The function generator was connected to

the computer via the USB port. To access and control the function generator it was first installed in windows so that it can be accessed by any application from the operating system.

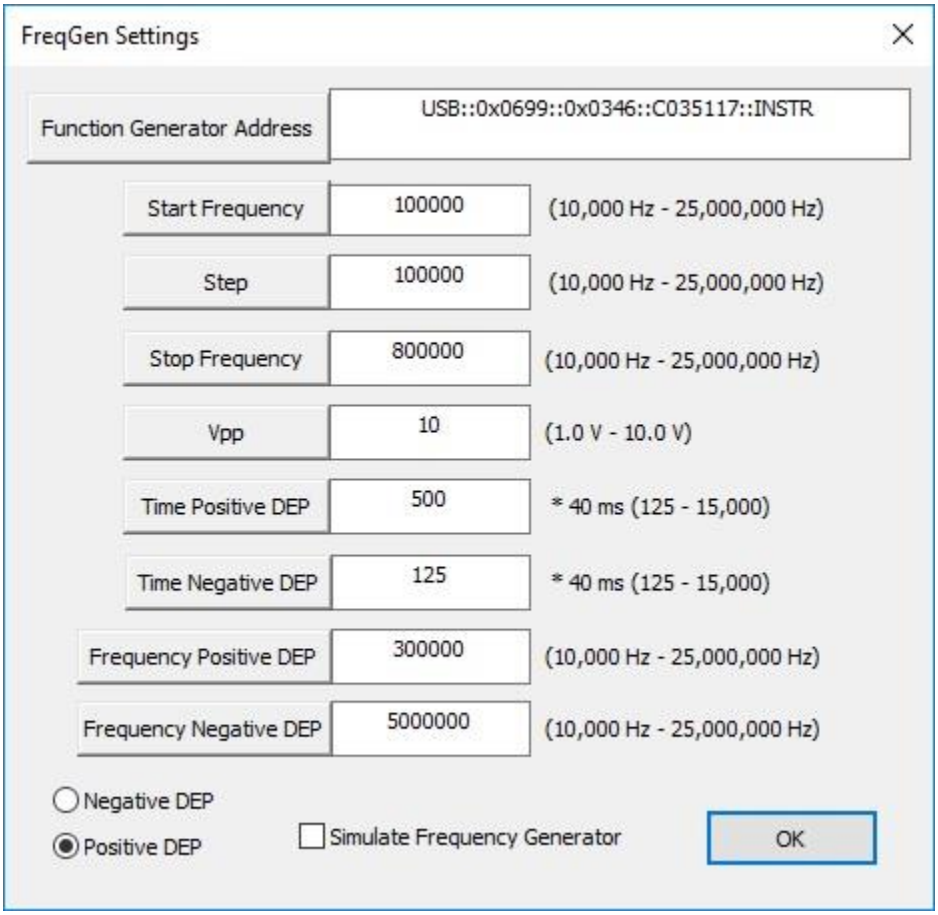

Fig. 9. Function Generator Settings dialog window

That task was accomplished by installing a Virtual Instrument Software Architecture (VISA) software. VISA is an industry wide standard architecture and has many proprietary implementations. Since I am using the Tektronix AFG series function generator so I have used TekVISA connectivity software that was provided by Tektronix. After installation of TekVISA connectivity software I was able to control the function generator from the TekVISA software interface through Tektronix provided user commands. Now, the next step was to interface between TekVISA and the Visual C++ application. The Tektronix user commands were not recognized in

Visual C++ environment. For that purpose, I modified an Interchangeable Virtual Instruments Foundation (IVI) compliant device driver from LabWindows™/CVI environment to Microsoft Visual C++. The IVI foundation is an industry wide consortium that maintains a software repository and helpful guides for access and control of laboratory and testing equipment. IVI compliant drivers for LabVIEW were easily available for download. However, since Visual C++ is not as widely adopted as LabVIEW to interface with instruments, there was no available compatible driver for Visual C++ in the IVI online software repository. The best driver I found was coded for LabWindows™/CVI which is an ANSI C integrated development environment (IDE) by National Instruments. To use this driver in Visual C++ some commands were needed to be modified and the driver had to be compiled in Microsoft Visual Studio. This modified device driver along with TekVISA connectivity software was used to access and control the function generator from Microsoft Visual C++ program. The section of the code that access and controls the function generator is included in Appendix A.

Fig. 10. Delete Results Confirmation dialog window

Once all the settings are completed, the “Start Experiment” button may be clicked to start the experiment and start recording images and results. The experiment automatically stops when the stop frequency is reached. The experiment can also be stopped by clicking the “Stop Experiment” button. Moreover, in addition to the automatically saved images and recorded results, an image or result at any instance can be saved by clicking “Save Image” and “Save Result”

buttons. The “Delete Results” button in Fig. 6 is utlized if, for any reason, the experiment was not properly conducted and the results need to be deleted. Before deleting any results, a confirmation dialog as shown in Fig. 10 is displayed to prevent the accidental deletion of valuable experimental data.

The program can be closed by clicking the cross in the upper right corner of the dialog window in Fig. 5. I have ensured to free all the reserved resources during program execution before exiting the program to avoid any memory leaks.

4. EXPERIMENTAL SETUP

The experimental setup used for the project is displayed in the Fig. 11. It consisted of a personal computer with windows operating system, an OMFL600 low power microscope, pearl – shaped interdigitated (PID) electrode, UVC compliant ProScope PS-MC5UW microscope camera and Tektronix AFG3021B function generator. The custom-built side illumination system is also displayed in Fig. 11. The operational detail of the side illumination system is presented in chapter 7 of the dissertation. The OMFL600 microscope was placed on an optical table top purchased from Newport Corporation to dampen any vibrational noise.

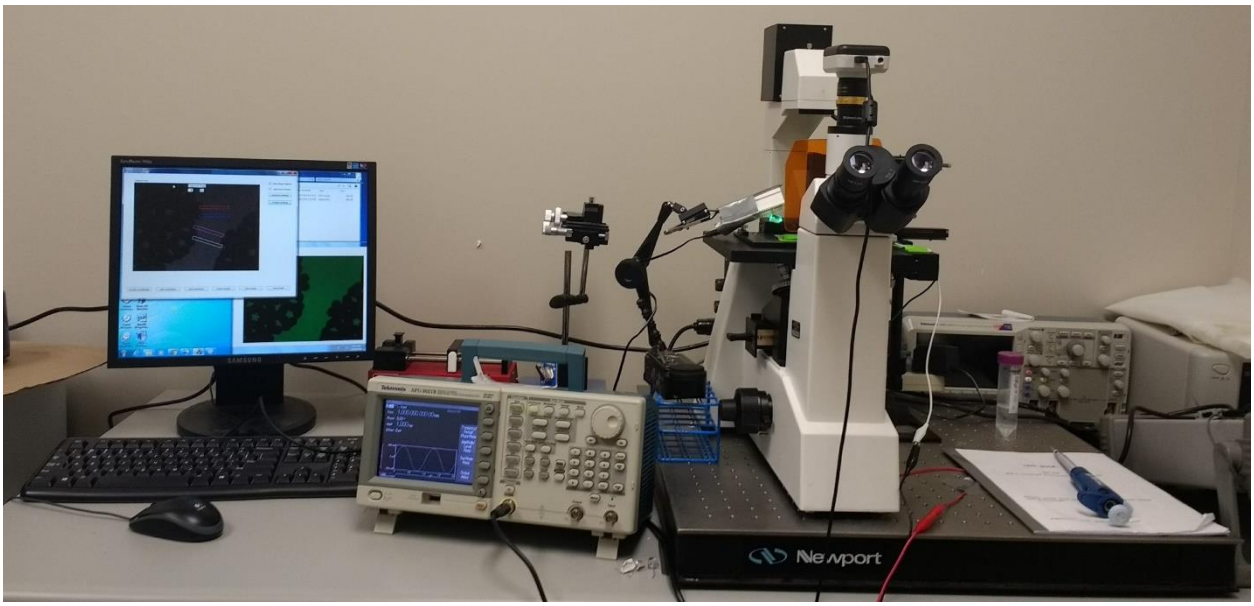

Fig. 11. Experimental Setup for the project

DEP spectroscopy application is installed and run on a personal computer with windows operating system. A UVC compliant ProScope PS-MC5UW microscope camera and a Tektronix AFG3021B function generator were connected to the personal computer through USB port. The sample containing the rare analytes was pipetted onto the PID electrode for observation and recording of data during the experiment. Fig. 12 shows the close-up top view of the PID electrode

placed on the OMFL600 microscope. The objective lens of the microscope is visible below the PID electrode. The terminals of the electrode were connected to the output port of the Tektronix AFG3021B function generator.

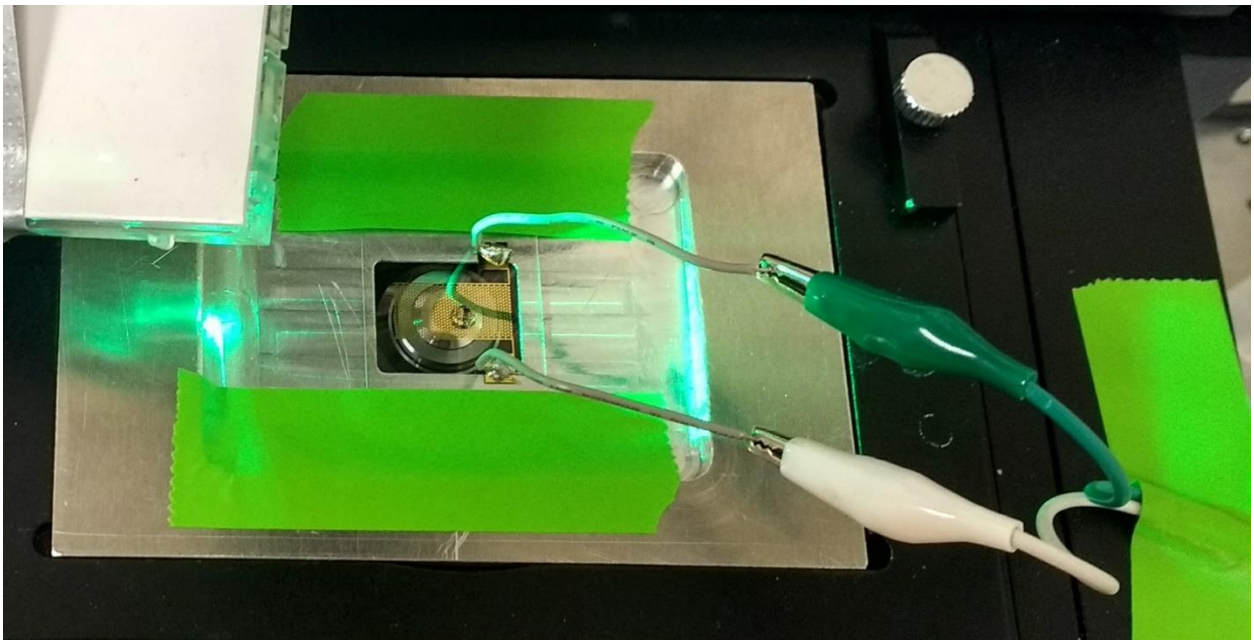

Fig. 12. PID electrode placed on OMFL600 low-power microscope for observation. Electrode terminals are connected to the Tektronix AFG3021B function generator.

The PID electrode was affixed in place by the adhesive tape to eliminate any chance of accidental movement during the experiment.

5. DEP CROSSOVER FREQUENCY MEASUREMENT

The automated software was validated by measuring the crossover frequency and DEP spectrum of blue colored polystyrene beads purchased from Sigma-Aldrich. The nominal diameter of the polystyrene beads with dark blue dye was 1000 nm. The experiemnt was performed with PID electrode that was designed in the Biomedical Engineering Laboratory at NDSU and fabricated in the NDSU microfabrication facilities. The electrode was designed and drawn to scale in AutoCAD, validated in COMSOL Multiphysics and fabricated on a commercially available glass wafer using photolithography, metal sputtering and lift-off procedures using 1000Å thick gold film. The PID electrode is capable of generating the maximum electric field of 1.8×10^4 V/m, which is sufficient to polarize the polystyrene beads for microscopic observation of DEP. It was reported earlier in Ref. 5 that the average electric field and the electric field gradients do not vary with frequency in the PID electrode. This ensured that the polystyrene beads are subjected to the same electric field gradients at all frequencies, and their DEP behavior is only dependent on the value of $Re[K_{CM}(\omega)]$, which is dependent on the polarizability of the beads and the medium.

The variation of the DEP force on 1000 nm polystyrene beads with dark blue dye was observed at various frequencies. I took 10 µL polystyrene beads with a pipette in a centrifuge tube and centrifuged at 5000 rpm for 12 minutes to separate the beads from the solution. After centrifugation, the supernatant was removed and 390 µL of 0.01X diluted phosphate buffer saline (PBS) with conductivity 0.01 S/m was added. The 10 µL of the prepared bead solution was pipetted onto the clean PID electrode which was mounted on an OMFL600 low-power microscope for observation during the experiment. The UVC compliant ProScope PS-MC5UW microscope camera fitted on the top of the microscope was connected to the computer running the DEP spectroscopy application to observe the PID electrode. The PID electrode was connected to a

Tektronix AFG 3021B function generator. The function generator was also connected to the DEP spectroscopy application for automated frequency switching during the experiment. The sample on the electrode was illuminated by the mercury arc lamp of the microscope.

Fig. 13. The camera feed in DEP spectroscopy application with regions of interest marked by red (for negative dielectrophoresis) and blue (for positive dielectrophoresis) rectangles[51]

DEP spectroscopy application software was used for observation and recording of the results during the experiment. Two regions of interest were identified and selected as shown in Fig. 13. The red rectangle marks the area of low electric field strength where polystyrene beads are collected in the case of negative dielectrophoresis. In case of positive dielectrophoresis the polystyrene beads are attracted to the high electric field regions towards the edge of the electrodes.

The formation of a bridge or chain of polystyrene beads was observed between the opposite edges of the electrode in the experiment in the case of positive dielectrophoresis as shown in Fig. 14. The blue rectangle to mark the region of interest for positive dielectrophoresis was placed to capture this effect. To start recording the measurements, the Start Experiment button in the software measurement window was clicked. At the beginning, the function generator was automatically set to a positive frequency of 50 kHz to establish positive DEP.

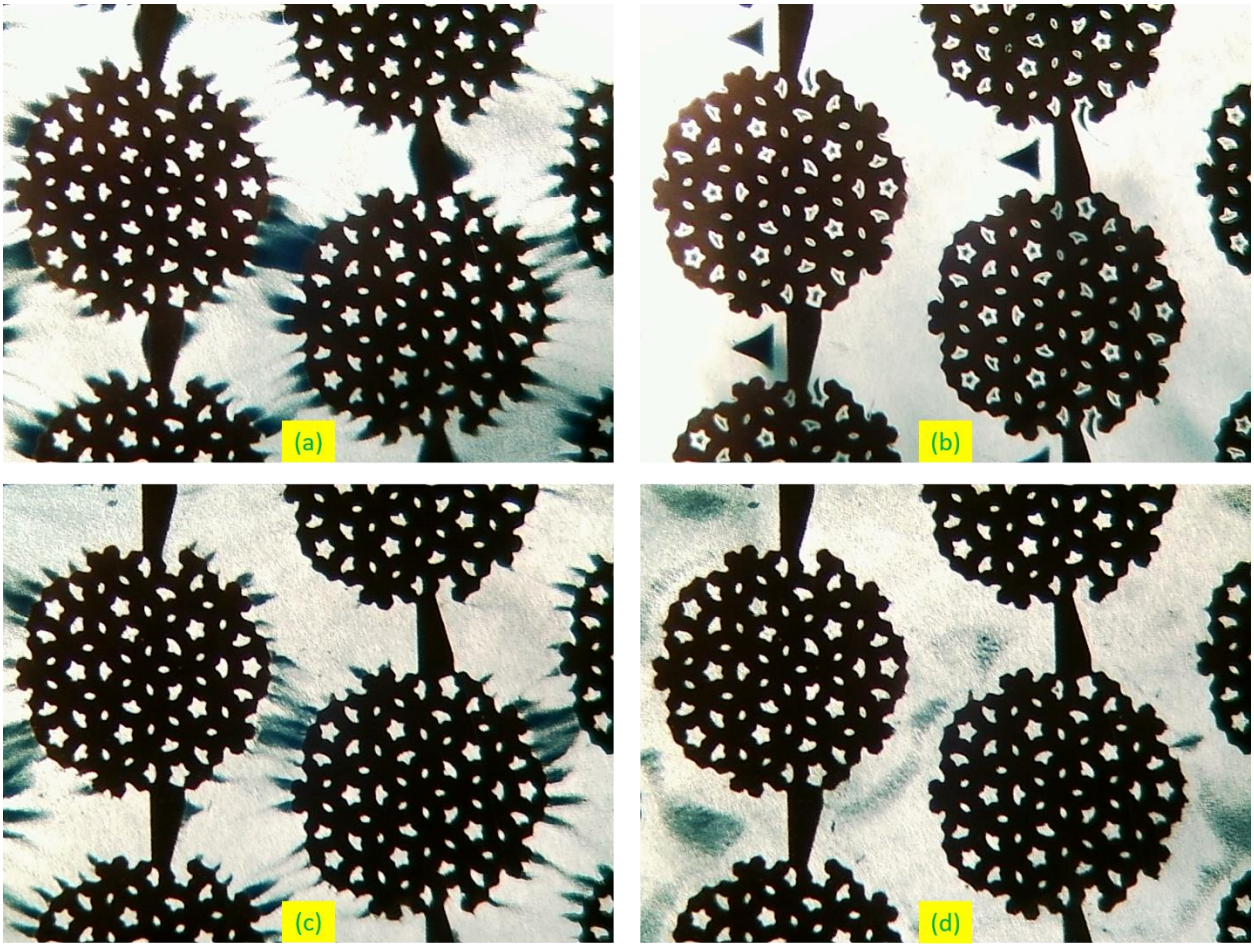

Fig. 14. DEP effect with blue polystyrene beads of 1000 nm diameter (a) Positve DEP effect observed with applied electric field frequency of 100 kHz (b) Negative DEP effect observed with applied electric field frequency of 15000 kHz (c) Positive DEP effect obsereved with applied electric field frequency of 400 kHz (d) Negative DEP effect observed with applied electric field frequency of 500 kHz.[51]

Through earlier trial experiments, it was observed that low frequency electric fields (<100 kHz) induce a positive DEP force whereas high frequency electric fields (> 1000 kHz) induce a negative DEP force for the polystyrene beads suspended in the PBS buffer. The positive DEP force resulted in the attraction of the beads towards the edge of the electrodes, and they formed a bridge or chain between the opposite ends as shown in Fig. 14. The collection of the beads in the regions of interest decreases the average light intensity in that region. For example, in case of negative dielectrophoresis, the negative region of interest is much darker in color as compared to the positive region of interest and vice versa. This observation was utilized to measure the DEP crossover frequency and the spectroscopic curve.

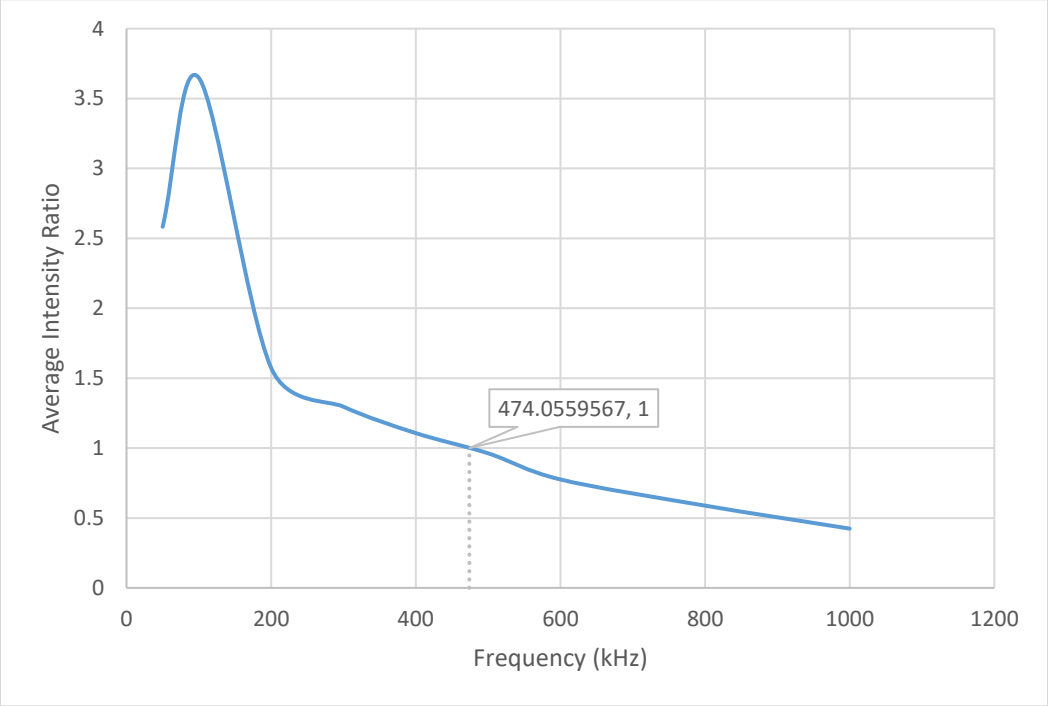

Fig. 15. Average intensity ratio (light intensity of negative DEP region / light intensity of positive DEP region) versus frequency of the applied electric field. The crossover frequency was found to be 474 kHz.[51]

The ratio of the average light intensity in the negative DEP region with the average light intensity in the positive DEP region was calculated and plotted against the frequency of the applied

electric field. At the crossover frequency, the beads should be uniformly distributed across the sample because of diffusion through Brownian motion. So, the average light intensity in both the regions would be the same and their ratio would be equal to one. The crossover frequency was found to be 474 kHz from the DEP spectroscopic curve as shown in Fig. 15.

The measurements were recorded after an interval of about 2 minutes to ensure that the beads were collected at their respective high or low electric field regions. The Brownian motion of the beads was negligible as compared to the DEP force as was predicted in Ref. 42. The drag force experienced by the polystyrene beads was also negligible since the beads had been settled in their respective regions and any negligible movement observed was caused by the Brownian motion. However, the rise in temperature because of the high applied electric field (1.8×10^4 V/m) resulted in temperature rises that caused generation of electrothermal forces and evaporation of the sample. This drawback limited the time of the experiment. To overcome this drawback, it was sought to optimize the code for faster execution.

6. DEP SPECTROSCOPY

Some experiments were also performed with fluorescent polystyrene beads of 500 nm nominal diameter that were purcahsed from Phosphorex Inc. The DEP spectroscopy application was used to calculate the DEP crossover frequency and the positive and negative DEP spectrum of these fluorescent polystyrene beads.

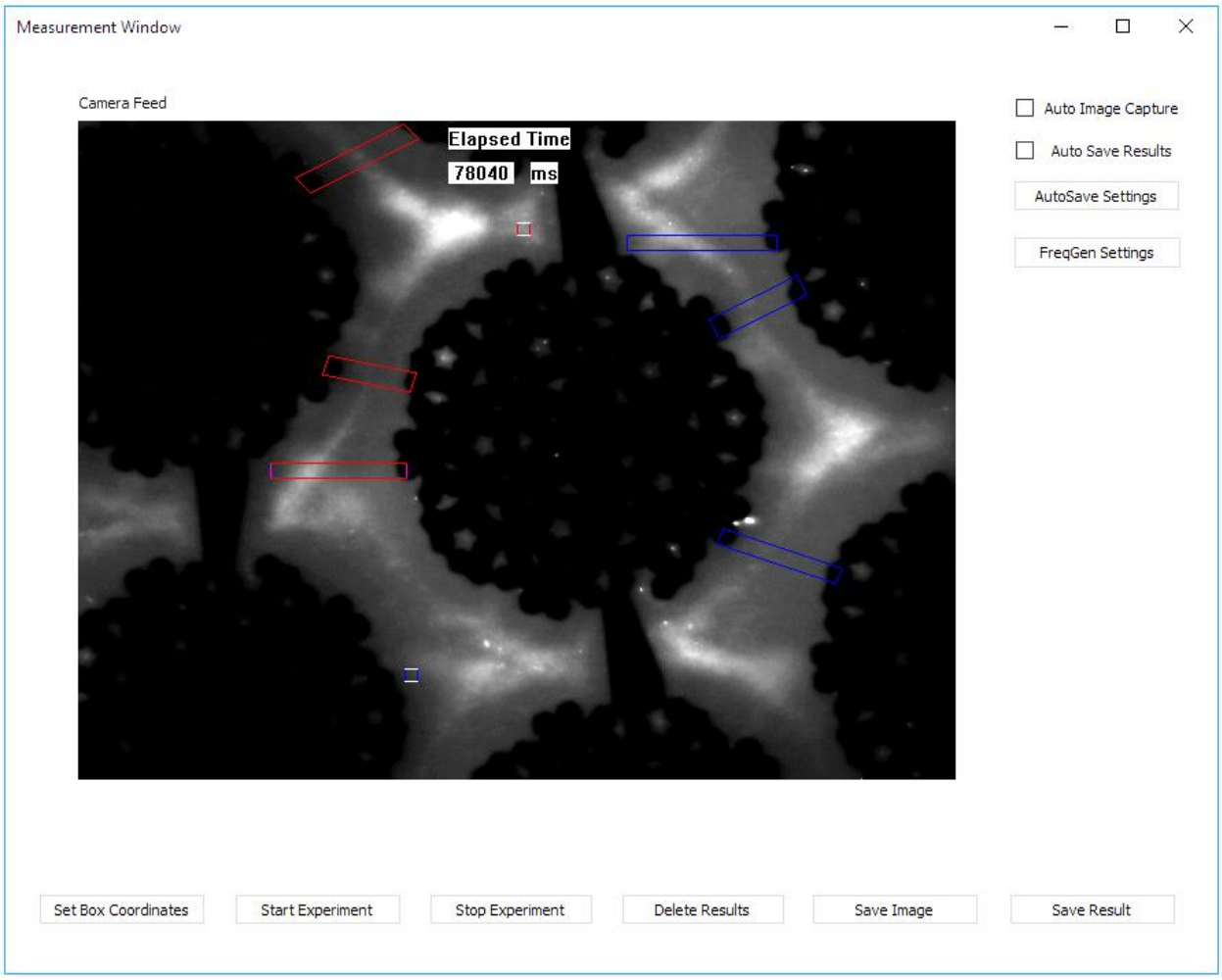

Fig. 16. Measurement Window of DEP spectroscopy application with marked regions of interest[51]

The experiemnt was performed with the same PID electrode that was designed and fabricated by our research group. The variation of DEP force on 500 nm fluorescent polystyrene beads was observed at various frequencies. The 10 µL polystyrene beads were taken with a pipette

in a centrifuge tube and centrifuged at 5000 rpm for 12 minutes to separate the beads from the solution. After centrifugation, the supernatant was removed and 390 µL of 0.01X diluted phosphate buffer saline (PBS) with conductivity 0.01 S/m was added. The 10 µL of the prepared bead solution was pipetted onto the clean PID electrode which was mounted on OMFL600 low power microscope for observation during the experiment. Then the UVC compliant ProScope PS-MC5UW microscope camera fitted on the top of the microscope was connected to the computer running the DEP spectroscopy application.

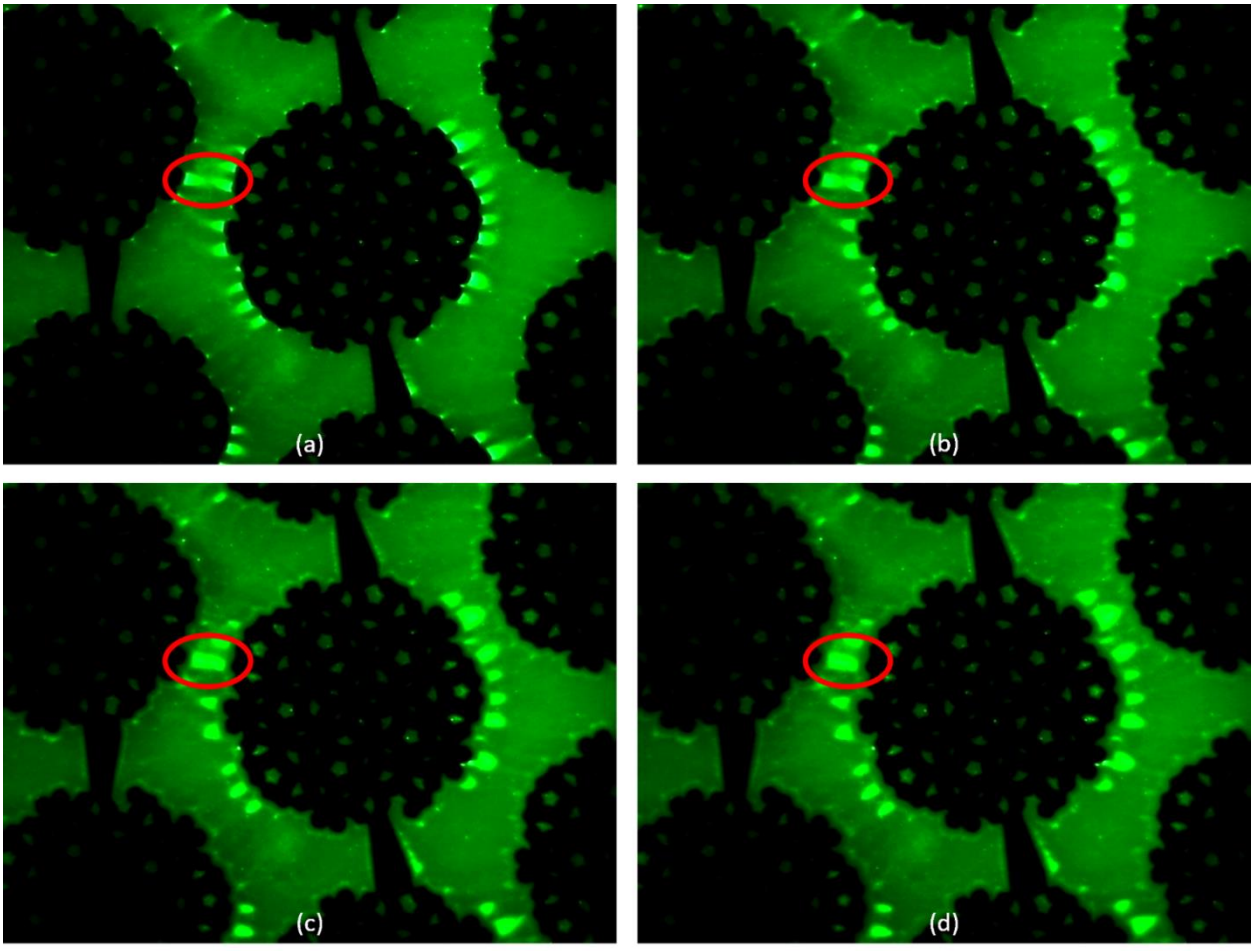

Fig. 17. Demonstration of positive and negative DEP effect through time – lapse images captured through DEP spectroscopy application (a) Beads are collected at the edge of the electrode due to positive DEP. (b) At the instant when electric field intensity is changed to induce negative DEP (c) 80 ms later (d) 160 ms later.[51]

The PID electrode was connected to Tektronix AFG 3021B function generator. The function generator was also connected to the DEP spectroscopy application for automated frequency switching during the experiment. The sample on the electrode was illuminated by the green fluorescent lamp with excitation wavelength of 460-550 nm and emission wavelength of 590 nm.

DEP spectroscopy application software was used for observation and recording of the results during the experiment. For this experiment, the software was modified to mark six regions of interest along with two smaller squares to mark background noise as shown in Fig. 16. In each region of interest, the fluorescence intensity was calculated. The fluorescence intensity in the two background boxes was also calculated and their average was used as background noise to calculate the DEP spectroscopic curve.

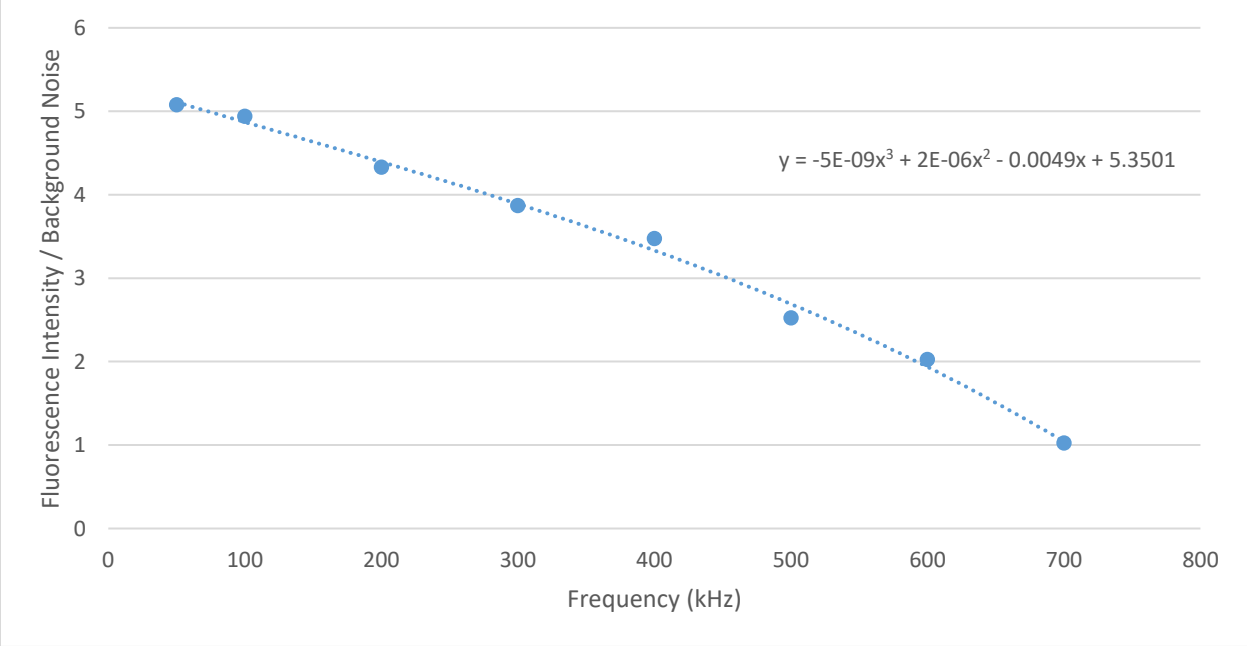

Fig. 18. Positive DEP spectroscopy curve. Crossover frequency is 719.25 kHz.[51]

For positive DEP, the fluorescent polystyrene beads accumulated in the same way as was in the previous experiment with polystyrene beads with blue color dye. The beads were attracted

to the edges of the electrode and formed a bridge or chain between the two opposite sides in the high electric field region as shown in Fig. 17. The recorded fluorescence intensity values from a region of interest and average of intensity in the two background boxes was used to calculate the DEP spectroscopy curves. The ratio of the fluorescence intensity and the background noise was plotted against the applied frequency of the electric field to obtain the positive DEP spectroscopy curve as shown in Fig. 18. At the crossover frequency f_{xo}, the DEP force F_{DEP} is zero, so the fluorescent polystyrene beads diffuse throughout the sample because of Brownian motion. This should result in the observation of same fluorescence intensity all over the sample. Hence, the ratio of fluorescent intensity in the region of interest to the background noise should be equal to one for the crossover frequency. The positive DEP spectroscopy curve was extrapolated as shown in Fig. 18 to find out the crossover frequency. For this experiment the crossover frequency was found to be 719.25 kHz[51].

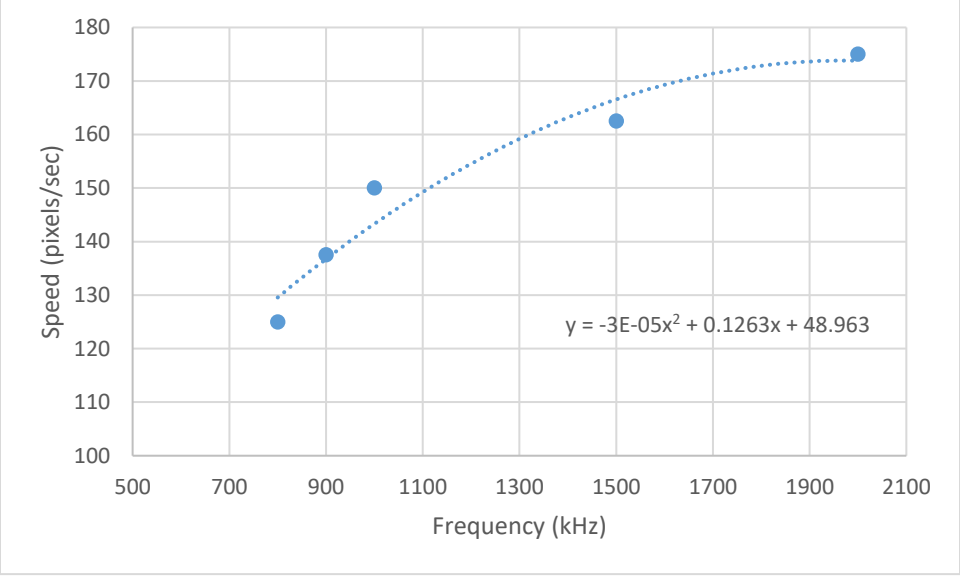

Fig. 19. Negative DEP spectroscopy curve. Each pixel corresponds to 0.6 µm.[51]

However, in this experiment, a precise collection of the fluorescent polystyrene beads in the low electric field region was not observed during negative DEP. This issue pushed us to devise

a new strategy to observe and quantify negative DEP effect. Here it was observed that as the applied electric field frequency is switched to induce negative DEP, the fluorescent polystyrene beads attached to the electrode edges are repelled from the electrode and disperse in the medium as shown in Fig. 17. The speed of repulsion of these fluorescent polystyrene beads was calculated and plotted against the applied frequency of the electric field to obtain the negative DEP spectroscopy curve as shown in Fig. 19. The crossover frequency from the negative DEP spectroscopy curve cannot be found since the speed of the fluorescent polystyrene beads would never be zero. Even at the crossover frequency, there should be some motion of the beads because of the diffusion through Brownian motion.

The Brownian motion was negligible as compared to the DEP force as was predicted in Ref. 42. The drag force due to the friction of the fluid arises in the observation of the negative DEP spectroscopy. It opposed the repulsion of the beads from the edge of the electrode. The rise in temperature of the sample because of the heat dissipation due to the applied electric field in a very small volume was also observed. This rise in temperature resulted in generation of electrothermal forces and the evaporation of the sample. This shortcoming limited the time of the experiment and posed a challenge in achieving higher spectral resolution of the DEP spectroscopy curve.

7. RARE ANALYTE QUANTIFICATION THROUGH NEGATIVE DEP SPECTROSCOPY

The variation of the DEP force on biotin-avidin conjugated polystyrene beads at various frequencies was also studied. The biotin functionalized polystyrene beads with 0.74 µm diameter (10,000 biotin molecules on each bead surface) were purchased from Spherotech Inc. These biotinylated beads were conjugated with fluorescently labelled avidin molecules (1 mg/ml) purchased from Vector Labs Inc. using the procedure recommended by the manufacturer.

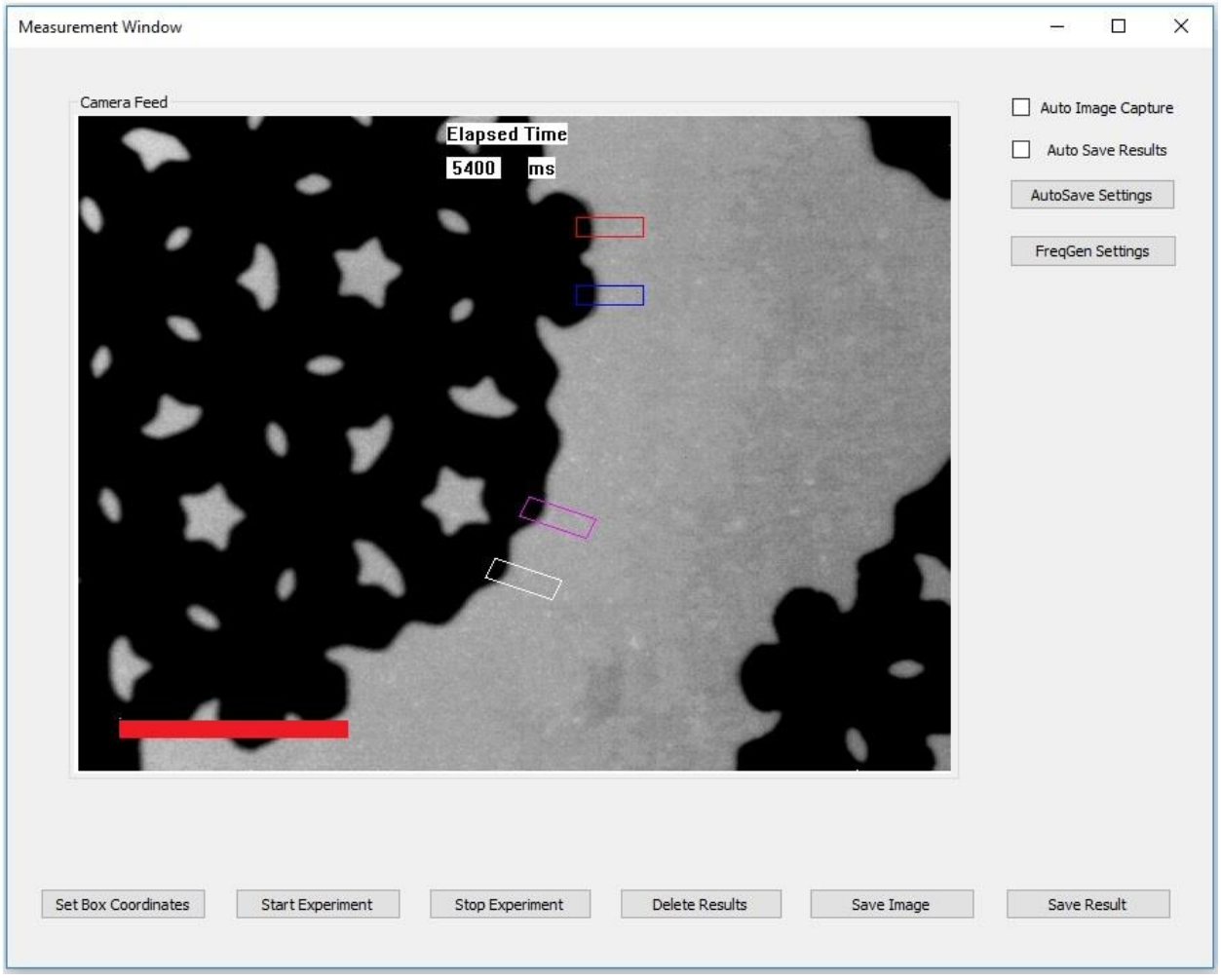

Fig. 20. Microsoft Windows application for DEP Spectroscopy. The regions of interest are marked with colored rectangles. PID electrode is visible as darker region in the picture. Scale bar indicates 100 µm.[52]

To achieve 100% avidin-biotin conjugation (i.e. 10,000 biotin molecules on the surface of polystyrene beads attached to 10,000 avidin molecules) 3µL of avidin solution and 10 µL biotin functionalized polystyrene beads were incubated for 30 min at room temperature. The solution was then centrifuged at 5000 rpm for 12 min to separate functionalized beads from the solution. After centrifugation, the supernatant was removed and 390 µL of 0.01X diluted phosphate buffer saline (PBS) with conductivity 0.01 S/m was added. The 10 µL of the prepared conjugated bead solution was pipetted onto the PID electrode for microscopic observation during the experiment. Similarly, 50% and 0.8% avidin-biotin conjugated solutions were prepared by diluting the avidin solution appropriately and keeping other parameters (incubation time, temperature, and centrifuge speed) constant. The 0% solution contained only biotin functionalized polystyrene beads.

For the experiment, a clean PID electrode was mounted on OMFL600 low power microscope and a side illumination technique for observations was employed. A custom made green LED lamp illuminating from an angle of incidence of 45 degrees was used. This angle of incidence reduces the amount of light collected by the camera that does not result from Rayleigh scattering from the beads. When 10 µL of the prepared beads solution was pipetted onto the electrode, the scattered light from the beads illuminated the electrode and is refracted towards the microscope objective resulting in a sharp image of the beads without the use of fluorescence. Since the diameter of the beads (~740 nm) is of the same order of magnitude as the wavelength of the green LED (565 nm), the beads appear very bright on a dark background due to Rayleigh scattering. The use of light source with a large incidence angle precluded the need of a complicated fluorescent enabled sample and fluorescent microscope for the experiment and introduced a simple and cost effective illumination for the microscopic observations. The PID electrode was connected to the Tektronix AFG 3021B function generator.

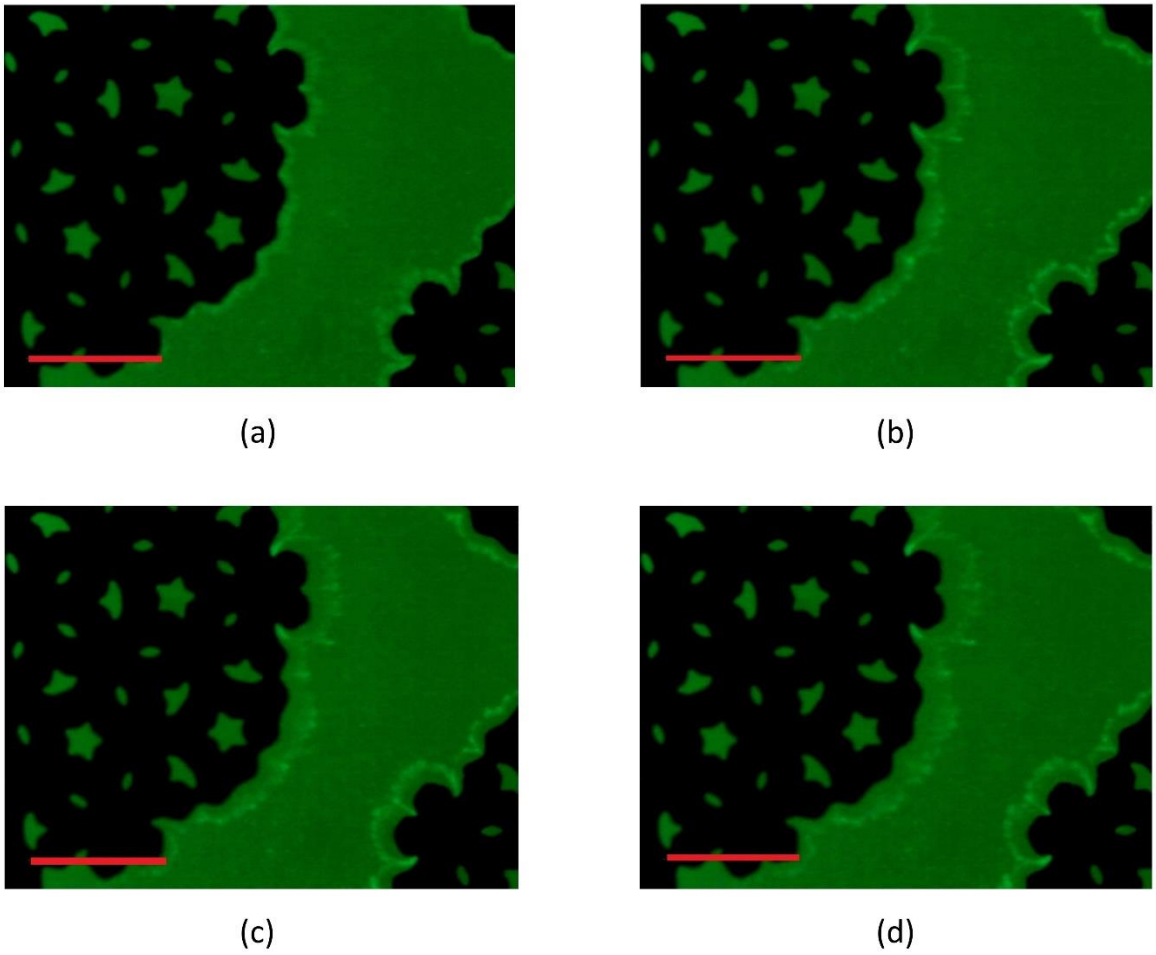

Fig. 21. Demonstration of negative DEP effect through time – lapse images captured through DEP spectroscopy application (Assuming time = 0 when electric field frequency is changed to induce negative DEP) (a) *t* = 0 ms (b) *t* = 80 ms (c) *t* = 160 ms (d) *t* = 240 ms. PID electrode is visible as darker region in the picture. Scale bar indicates 100 μm.[52]

DEP spectroscopy application software was used for observation and recording of the results during the experiment. To start the negative DEP spectroscopy measurement, the Start Experiment button in the software measurement window was clicked. At the beginning, the function generator was automatically set to a positive frequency of 10 kHz to establish positive DEP. Low frequency electric fields (< 50 kHz) induce positive DEP whereas high frequency electric fields (> 250 kHz) induce negative DEP force for the polystyrene beads suspended in the

PBS buffer[5]. The positive DEP force resulted in the attraction of the beads towards the edge of the electrodes. A clear line of bright white beads can be seen forming at the edge of the electrodes in Fig. 21(a). Once the beads form a layer at the edge of the electrode, the software automatically switched the frequency to another value to observe the negative DEP spectroscopy. The negative DEP force resulted in the quick repulsion of the beads from the edge of the electrode. The repulsion of the beads was tracked and recorded by the software.

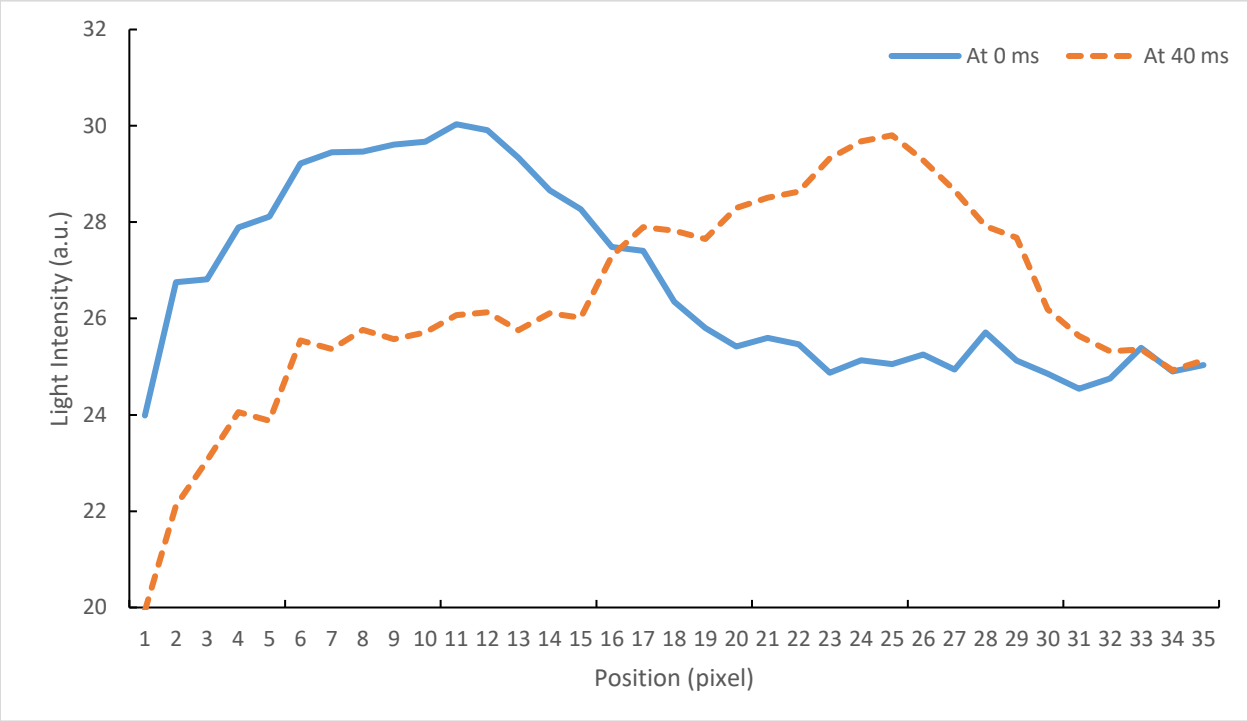

Fig. 22. Plot of the Light Intensity versus the Position in the region of interest. Each pixel corresponds to 0.6 μm.

The speed of the repulsed beads as the travel away from the electrode edge was calculated through image processing. The variation in light intensity in the region of interest was measured with respect to the horizontal position in the region of interest at different time intervals as shown in Fig. 22. The peak light intensity observed in the image corresponds to the position of the functionalized beads. Two images were processed to calculate the speed of repulsion, one captured

at positive DEP and the other just after switching to negative DEP. The shift in the center of the mass of the light intensity is calculated for both images and is used to find out the speed of the repulsion due to negative DEP.

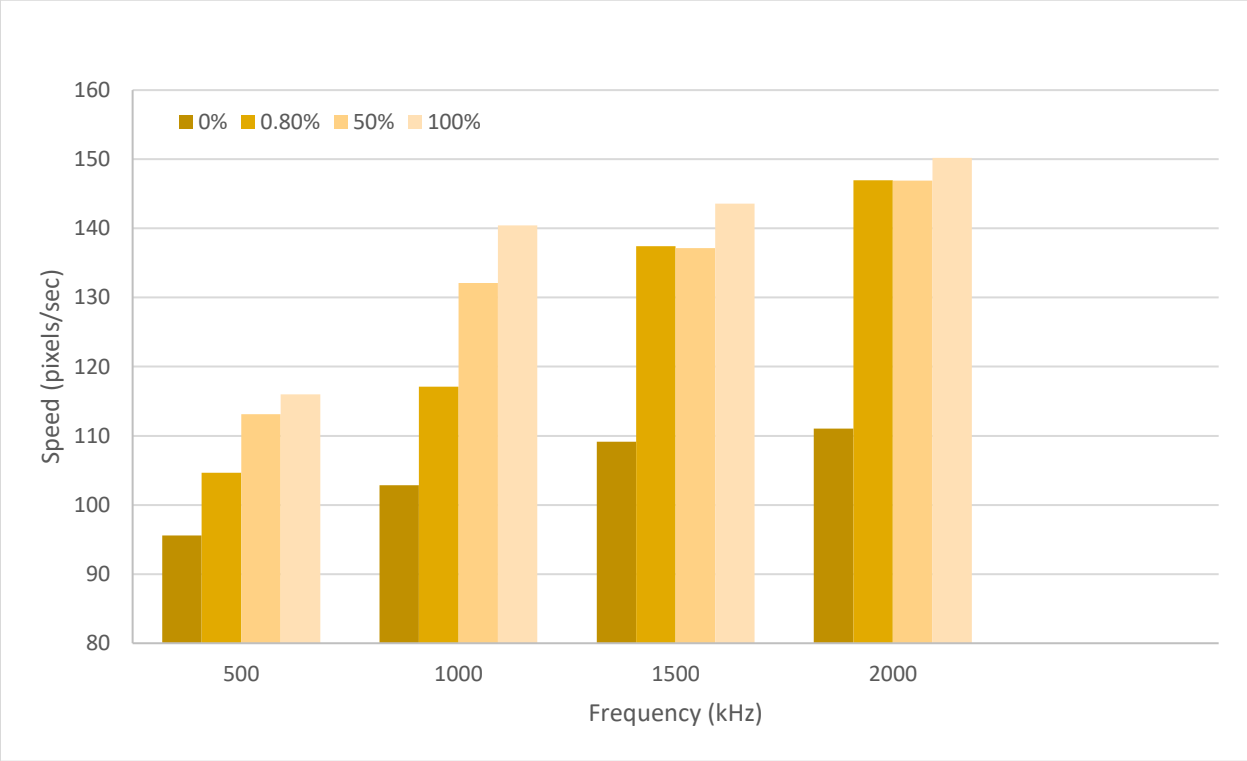

Fig. 23. DEP Spectroscopic Curve. Each pixel corresponds to 0.6 μm.

A relationship between the speed of repulsion of the beads and the applied frequency of the electric field was observed. As the software switched to higher frequency electric fields, the negative DEP force was increased resulting in a higher speed of repulsion from the edge of the electrode. While switching the frequency, all other experiment parameters and conditions were maintained and kept constant. The obtained DEP spectroscopy results are shown in Fig. 23. A significant change in the repulsion speed of the beads between 0% avidin-biotin conjugation (i.e. only biotin functionalized polystyrene beads) and 0.8 % conjugation (80 avidin molecules attached per biotin functionalized polystyrene bead) was observed, especially in the frequency range above

1500 kHz. This means that this experimental setup can detect as little as 80 avidin molecules attached on the biotin functionalized polystyrene bead surface[52].

The Brownian motion was negligible as compared to the DEP force. However, the high electric field in a small volume resulted in increase in temperature due to heat dissipation. This increased temperature gave rise to generation of electrothermal forces and eventual evaporation of the sample. Another limitation encountered was that the PID electrode was made up of gold and biotin has affinity for gold[53–57]. After a few readings, the biotinylated polystyrene beads were adsorbed onto the electrode. This required frequent cleaning of the PID electrode for further observations.

The polystyrene beads also experience hydrodynamic drag force due to friction which is opposite in direction to the DEP force. Since the hydrodynamic drag force also depends on the size of the particle, biotin functionalized polystyrene beads with higher concentrations of attached avidin experienced higher drag force. The observed increase in speed for these beads means that the increase in DEP force was greater than the increase in the hydrodynamic drag force. The graph in Fig. 23 can be considered as a calibration curve for sensing and identification of avidin in biological samples in a medium with the same conductivity.

8. OPTIMIZATION OF DEP SPECTROSCOPY APPLICATION AND RECOMMENDATIONS FOR IMPROVED ELECTRODE DESIGN

It has been recommended to improve the design of the electrode and the experimental procedure to achieve better spectral resolution of negative dielectrophoretic spectroscopy to further lower the detection limit of rare analytes in a biological sample. Although, the current PID electrode provided high electric field gradients to polarize the polystyrene beads for dielectrophoretic spectroscopy but its complex design made it difficult to predict the regions of interest where polystyrene beads could be observed in the case of positive or negative DEP. So, it is recommended to design and fabricate another electrode with simpler geometry that can provide similar high electric field gradients with more predictable regions of interest where polystyrene beads could be collected and observed in the case of positive or negative DEP. Such an electrode will result in simpler algorithms to analyze the results through DEP spectroscopy application and will improve the spectral resolution and reliability of the DEP spectroscopy curve.

The DEP spectroscopy application is also optimized for faster execution to complete the data collection process before the generation of electrothermal forces in the observed sample. Initially, images and results were saved to the hard disk during the program execution. It took much longer to execute the program since, writing to hard disk is a slower process as compared to saving the data in computer memory. In the latest version of the program that I developed, all the data is stored in memory until the end of experiment and saved later before closing the program. Moreover, the data collection strategy has been revised and streamlined to save only the required results in memory rather than keeping all the captured images during the experimental procedure. This improvement also reduced the amount of data to be stored in memory, reducing the risk of an error due to insufficient computer memory. Once the spectral resolution of the negative

dielectrophoretic spectroscopy is increased through improved electrode design and optimized software application, it is being planned to design and test a complete point of care system for detection and quantification of rare analytes in biological samples using this method.

9. CONCLUDING REMARKS

I have proposed and validated an automated technique for detection and quantification of rare analytes in biological samples. I have tested the technique with detection and quantification of avidin conjugated to biotin functionalized polystyrene beads. This technique can be extended for detection and quantification of other rare analytes through careful selection of binding antibodies. For example, to diagnose myocardial infarction, troponin needs to be detected. This can be accomplished by using an antibody that binds troponin instead of using biotin functionalized polystyrene beads. It can help physicians to save many human lives from life threatening diseases like cancer and myocardial infarction. I was able to achieve an improvement by an order of magnitude in the detection limit of rare analytes when compared to previously published results[5]. I have also optimized the DEP spectroscopy application to achieve higher spectral resolution of negative dielectrophoretic spectroscopy. My technique has the potential to be incorporated into a point of care lab on chip device because of its use of very small electrodes and automated software for detection and quantification of biomolecules that are indicators of diseases.

REFERENCES

1. L. M. Broche et al., “Early detection of oral cancer – Is dielectrophoresis the answer?,” Oral Oncol. **43**(2), 199–203 (2007) [doi:10.1016/j.oraloncology.2006.02.012].
2. J. F. Rusling et al., “Measurement of biomarker proteins for point-of-care early detection and monitoring of cancer.,” Analyst **135**(10), 2496–2511, NIH Public Access (2010) [doi:10.1039/c0an00204f].
3. J. S. Daniels and N. Pourmand, “Label-free impedance biosensors: Opportunities and challenges,” in Electroanalysis **19**(12), pp. 1239–1257, NIH Public Access (2007) [doi:10.1002/elan.200603855].
4. R. Pethig and S. Smith, *Introductory Bioelectronics: For Engineers and Physical Scientists*, in Introductory Bioelectronics: For Engineers and Physical Scientists, Wiley (2012) [doi:10.1002/9781118443293].
5. L. Velmanickam, D. Laudenbach, and D. Nawarathna, “Dielectrophoretic label-free immunoassay for rare-analyte quantification in biological samples,” Phys. Rev. E **94**(4), 42408 (2016) [doi:10.1103/PhysRevE.94.042408].
6. B. V. Chikkaveeraiah et al., *Electrochemical immunosensors for detection of cancer protein biomarkers*, in ACS Nano **6**(8), pp. 6546–6561, American Chemical Society (2012) [doi:10.1021/nn3023969].
7. J. Wu et al., “Biomedical and clinical applications of immunoassays and immunosensors for tumor markers,” TrAC - Trends Anal. Chem. **26**(7), 679–688 (2007) [doi:10.1016/j.trac.2007.05.007].

8. H. Chen et al., “Protein chips and nanomaterials for application in tumor marker immunoassays,” in Biosensors and Bioelectronics **24**(12), pp. 3399–3411 (2009) [doi:10.1016/j.bios.2009.03.020].

9. A. A. Panackal et al., “Enzyme immunoassay versus latex agglutination cryptococcal antigen assays in adults with non-HIV-related Cryptococcosis,” J. Clin. Microbiol. **52**(12), 4356–4358 (2014) [doi:10.1128/JCM.02017-14].

10. I. C. Shekarchi et al., “Avidin-biotin latex agglutination assay for detection of antibodies to viral antigens,” J. Clin. Microbiol. **26**(5), 954–956 (1988).

11. J. a. Molina-Bolívar and F. Galisteo-González, “Latex Immunoagglutination Assays,” J. Macromol. Sci. Part C Polym. Rev. **45**(1), 59–98, Taylor & Francis Group (2005) [doi:10.1081/MC-200045819].

12. F. J. Gella, J. Serra, and J. Gener, “Latex Agglutination Procedures in Immunodiagnosis,” Pure Appl. Chem. **63**(8), 1131–1134 (1991) [doi:10.1351/pac199163081131].

13. H.-H. Chen et al., “High-purity separation of cancer cells by optically induced dielectrophoresis,” J. Biomed. Opt. **19**(4), 45002 (2014) [doi:10.1117/1.JBO.19.4.045002].

14. S. Gupta et al., “On-chip latex agglutination immunoassay readout by electrochemical impedance spectroscopy.,” Lab Chip **12**(21), 4279–4286 (2012) [doi:10.1039/c2lc40127d].

15. M. C. Rodriguez, A.-N. Kawde, and J. Wang, “Aptamer biosensor for label-free impedance spectroscopy detection of proteins based on recognition-induced switching of the surface charge.,” Chem. Commun. (Camb). **287**(34), 4267–4269, The Royal Society of Chemistry (2005) [doi:10.1039/b506571b].

16. M. Varshney et al., “A label-free, microfluidics and interdigitated array microelectrode-based impedance biosensor in combination with nanoparticles immunoseparation for detection of Escherichia coli O157:H7 in food samples,” Sensors Actuators, B Chem. **128**(1), 99–107 (2007) [doi:10.1016/j.snb.2007.03.045].

17. H. Cai, T. M. H. Lee, and I. M. Hsing, “Label-free protein recognition using an aptamer-based impedance measurement assay,” Sensors Actuators, B Chem. **114**(1), 433–437 (2006) [doi:10.1016/j.snb.2005.06.017].

18. Z. Zou et al., “Functionalized nano interdigitated electrodes arrays on polymer with integrated microfluidics for direct bio-affinity sensing using impedimetric measurement,” Sensors Actuators, A Phys. **136**(2), 518–526 (2007) [doi:10.1016/j.sna.2006.12.006].

19. R. Pethig, “Dielectrophoresis: Status of the theory, technology, and applications,” Biomicrofluidics **4**(2), 22811, American Institute of Physics (2010) [doi:10.1063/1.3456626].

20. G. L. Hornyak et al., *Fundamentals of Nanotechnology*, CRC Press (2008) [doi:10.1109/MNANO.2009.934215].

21. T. B. Jones, “Basic Theory of Dielectrophoresis and Electrorotation,” IEEE Eng. Med. Biol. Mag. **22**(6), 33–42 (2003) [doi:10.1109/MEMB.2003.1304999].

22. J. Suehiro et al., “Quantitative estimation of biological cell concentration suspended in aqueous medium by using dielectrophoretic impedance measurement method,” J. Phys. D. Appl. Phys. **32**(21), 2814–2820, IOP Publishing (1999) [doi:10.1088/0022-3727/32/21/316].

23. H. Song and D. J. Bennett, “A semi-analytical approach using artificial neural network for dielectrophoresis generated by parallel electrodes,” J. Electrostat. **68**(1), 49–56 (2010) [doi:10.1016/j.elstat.2009.10.001].

24. P. M. Pilarski and C. J. Backhouse, “A method for cytometric image parameterization.,” Opt. Express **14**(26), 12720–12743 (2006).

25. G. Pesce et al., “Simultaneous measurements of electrophoretic and dielectrophoretic forces using optical tweezers,” Opt. Express **23**(7), 9363, Optical Society of America (2015) [doi:10.1364/OE.23.009363].

26. M. T. Wei, J. Junio, and D. H. Ou-Yang, “Direct measurements of the frequency-dependent dielectrophoresis force,” Biomicrofluidics **3**(1), 1–8 (2009) [doi:10.1063/1.3058569].

27. D. J. Bakewell, J. Bailey, and D. Holmes, “Real-time dielectrophoretic signaling and image quantification methods for evaluating electrokinetic properties of nanoparticles,” Electrophoresis **36**(13), 1443–1450 (2015) [doi:10.1002/elps.201400500].

28. N. R. Shanmugam, S. Muthukumar, and S. Prasad, “Ultrasensitive and low-volume point-of-care diagnostics on flexible strips – a study with cardiac troponin biomarkers,” Sci. Rep. **6**, 33423, Nature Publishing Group (2016) [doi:10.1038/srep33423].

29. A. K. Martin et al., “Troponin elevations in patients with chronic cardiovascular disease: An analysis of current evidence and significance.,” Ann. Card. Anaesth. **19**(2), 321–327 (2016) [doi:10.4103/0971-9784.179638].

30. M. A. Daubert and A. Jeremias, “The utility of troponin measurement to detect myocardial infarction: Review of the current findings,” Vasc. Health Risk Manag. **6**(1), 691–699, Dove Press (2010) [doi:10.2147/VHRM.S5306].

31. M. P. Hughes, “AC electrokinetics: applications for nanotechnology,” Nanotechnology **11**(2), 124–132 (2000) [doi:10.1088/0957-4484/11/2/314].

32. Y. Sato and K. Hishida, “Electrokinetic effects on motion of submicron particles in microchannel,” Fluid Dyn. Res. **38**(11), 787–802 (2006) [doi:10.1016/j.fluiddyn.2006.04.003].

33. M. P. Hughes and N. G. Green, “The Influence of Stern Layer Conductance on the Dielectrophoretic Behavior of Latex Nanospheres,” Academic Press (2002) [doi:10.1006/jcis.2002.8324].

34. P. R. C. Gascoyne and J. Vykoukal, “Particle separation by dielectrophoresis,” in Electrophoresis **23**(13), pp. 1973–1983, NIH Public Access (2002) [doi:10.1002/1522-2683(200207)23:13<1973::AID-ELPS1973>3.0.CO;2-1].

35. U. Lei and Y. J. Lo, “Review of the theory of generalised dielectrophoresis,” IET Nanobiotechnology **5**(3), 86 (2011) [doi:10.1049/iet-nbt.2011.0001].

36. L. Velmanickam and K. Nawarathna, “Dielectrophoretic cell isolation in microfluidics channels for high-throughput biomedical applications,” in 2016 IEEE International Conference on Electro Information Technology (EIT), pp. 302–306, IEEE (2016) [doi:10.1109/EIT.2016.7535256].

37. E. Papagiakoumou et al., “Evaluation of trapping efficiency of optical tweezers by dielectrophoresis.,” J. Biomed. Opt. **11**(1), 14035 (2015) [doi:10.1117/1.2165176].

38. B. P. Lynch, A. M. Hilton, and G. J. Simpson, “Nanoscale dielectrophoretic spectroscopy of individual immobilized mammalian blood cells.,” Biophys. J. **91**(7), 2678–2686, The Biophysical Society (2006) [doi:10.1529/biophysj.106.082412].

39. A. Castellanos et al., “Electrohydrodynamics and dielectrophoresis in microsystems: scaling laws,” J. Phys. D. Appl. Phys. **36**(20), 2584–2597, IOP Publishing (2003) [doi:10.1088/0022-3727/36/20/023].

40. T. Z. Jubery, S. K. Srivastava, and P. Dutta, “Dielectrophoretic separation of bioparticles in microdevices: a review.,” Electrophoresis **35**(5), 691–713 (2014) [doi:10.1002/elps.201300424].

41. M. Li et al., “A review of microfabrication techniques and dielectrophoretic microdevices for particle manipulation and separation,” J. Phys. D. Appl. Phys. **47**(6), 63001, IOP Publishing (2014) [doi:10.1088/0022-3727/47/6/063001].

42. A. Ramos et al., “Ac electrokinetics: a review of forces in microelectrode structures,” J. Phys. D. Appl. Phys. **31**(18), 2338–2353 (1999) [doi:10.1088/0022-3727/31/18/021].

43. P. Y. Weng et al., “Size-dependent dielectrophoretic crossover frequency of spherical particles,” Biomicrofluidics **10**(1), 11909 (2016) [doi:10.1063/1.4941853].

44. F. Camacho-Alanis and A. Ros, “Protein dielectrophoresis and the link to dielectric properties,” Stroke **7**(3), 353–371 (2015) [doi:10.1161/STROKEAHA.113.002813.Oxidative].

45. B. Yafouz, N. A. dib Kadri, and F. Ibrahim, “Dielectrophoretic manipulation and separation of microparticles using microarray dot electrodes,” Sensors (Basel). **14**(4), 6356–6369 (2014) [doi:10.3390/s140406356].

46. L. Cui, D. Holmes, and H. Morgan, “The dielectrophoretic levitation and separation of latex beads in microchips,” Electrophoresis **22**(18), 3893–3901, Wiley Subscription Services, Inc., A Wiley Company (2001) [doi:10.1002/1522-2683(200110)22:18<3893::AID-ELPS3893>3.0.CO;2-2].

47. N. G. G. and and H. Morgan*, “Dielectrophoresis of Submicrometer Latex Spheres. 1. Experimental Results,” American Chemical Society (1998) [doi:10.1021/JP9829849].

48. J. Voldman et al., “Holding forces of single-particle dielectrophoretic traps.,” Biophys. J. **80**(1), 531–541, Elsevier (2001) [doi:10.1016/S0006-3495(01)76035-3].

49. A. Md Rashedul Kabir et al., “Drag force on micron-sized objects with different surface morphologies in a flow with a small Reynolds number,” Polym. J. **47**(8), 564–570, Nature Publishing Group (2015) [doi:10.1038/pj.2015.29].

50. E. Schäffet, S. F. Nørrelykke, and J. Howard, “Surface forces and drag coefficients of microspheres near a plane surface measured with optical tweezers,” Langmuir **23**(7), 3654–3665 (2007) [doi:10.1021/la0622368].

51. S. A. M. Kirmani et al., “Dielectrophoretic Spectroscopy Using a Microscopic Electrode Array,” in SPIE Proceedings of Photonics West 2017, pp. 10068–33 (2017).

52. S. A. M. Kirmani et al., “Negative dielectrophoretic spectroscopy for rare analyte quantification in biological samples,” under Revis. Publ. SPIE J. Biomed. Opt. (2017).

53. P. M. Wolny, J. P. Spatz, and R. P. Richter, “On the adsorption behavior of biotin-binding proteins on gold and silica,” Langmuir **26**(2), 1029–1034 (2010) [doi:10.1021/la902226b].

54. L. Häussling et al., “Biotin-Functionalized Self-Assembled Monolayers on Gold: Surface Plasmon Optical Studies of Specific Recognition Reactions,” Langmuir **7**, 1837–1840 (1991) [doi:10.1021/la00057a001].

55. T. Lakshmipriya et al., “Signal enhancement in ELISA: Biotin-streptavidin technology against gold nanoparticles,” J. Taibah Univ. Med. Sci. **11**, 432–438 (2016) [doi:10.1016/j.jtumed.2016.05.010].

56. C. M. Pradier et al., “Comparison of different procedures of biotin immobilization on gold for the molecular recognition of avidin: An FT-IRRAS study,” Surf. Interface Anal. **34**(1), 67–71 (2002) [doi:10.1002/sia.1254].

57. C.-M. Yam et al., “Binding of Biotin to Gold Surfaces Functionalized by Self-Assembled Monolayers of Cystamine and Cysteamine: Combined FT-IRRAS and XPS Characterization.,” J. Colloid Interface Sci. **235**(1), 183–189 (2001) [doi:10.1006/jcis.2000.7362].

APPENDIX A. SOURCE CODE TO ACCESS FUNCTION GENERATOR

The following are selected lines of code of the DEP spectroscopy application that are used to access the function generator and change the frequency of the applied electric field during the experiments.

```
if (ChangeFreqFlag)
{
	//Change the signal from Frequency Generator (Tektronix AFG3021B)
	ViSession   tkafg3k;
	ViStatus    error = VI_SUCCESS;
	Flag02 = TRUE;
	if (SimulateFlag)
	{
		CString strx;
		strx.Format(L"%g kHz", Freq / 1000);
		AfxMessageBox(_T("Simulate Mode: Selected Frequency = ") + strx);
		checkErr(tkafg3k_InitWithOptions("USB::0x0699::0x0346::C036068::INSTR"
		, VI_TRUE, VI_FALSE, "Simulate=1", &tkafg3k));
	}
	else
		checkErr(tkafg3k_init("USB::0x0699::0x0346::C036068::INSTR", VI_TRUE,
		VI_FALSE, &tkafg3k));
```

```
        checkErr(tkafg3k_ConfigureOperationMode(tkafg3k, "1",
        TKAFG3K_VAL_OPERATE_CONTINUOUS));
        checkErr(tkafg3k_ConfigureOutputMode(tkafg3k, TKAFG3K_VAL_OUTPUT_FUNC));
        checkErr(tkafg3k_ConfigureStandardWaveform(tkafg3k, "1",
        TKAFG3K_VAL_WFM_SINE, G_Vpp, 0.0, Freq, 0.0));
        checkErr(tkafg3k_ConfigureOutputEnabled(tkafg3k, "1", VI_TRUE));

Error:
        if (error != VI_SUCCESS)
        {
                ViChar   errStr[2048];
                tkafg3k_GetError(tkafg3k, &error, 2048, errStr);
                AfxMessageBox((CString)errStr);
        }
        if (tkafg3k)
                tkafg3k_close(tkafg3k);
}
```